F. A. Robinson, J. D. Foden, and A. S. Collins
Zircon geochemical and geochronological constraints on contaminated and enriched mantle sources beneath the Arabian Shield, Saudi Arabia
The Journal of Geology, 2015; 123(5):463-489

Published version at http://dx.doi.org/10.1086/683192

Zircon Geochemical and Geochronological Constraints on Contaminated and Enriched Mantle Sources beneath the Arabian Shield, Saudi Arabia

F. A. Robinson,[1,*] *J. D. Foden,*[2] *and A. S. Collins*[2]

1. Department of Geological Sciences, Stockholm University, Svante Arrhenius väg 8, SE-106 91 Stockholm, Sweden; 2. Centre for Tectonics, Resources and Exploration (TRaX), Department of Earth Sciences, University of Adelaide, Adelaide, South Australia 5005, Australia

ABSTRACT

Arabian Shield granitic zircon geochemistry provides insight into the petrogenetic processes involved in generating one of the planet's largest tracts of juvenile Neoproterozoic crust. New zircon geochemistry supports previous U-Pb and whole-rock data that defined four magmatic groups: (1) ~870–675 Ma island arc and synorogenic I-type granitoids (IA+Syn), (2) ~640–585 Ma I- and A-type granitoids from the Nabitah and Halaban Suture (NHSG), (3) ~610–600 Ma postorogenic perthitic (hypersolvus) A-type granitoids (POPG), and (4) <600 Ma anorogenic aegirine–bearing perthitic (hypersolvus) A-type granitoids (AAPG). The low Nb (~1–300 ppm) and intrasuite rare earth element variation in IA+Syn and NHSG zircons indicates that these suites are derivatives of contaminated mantle followed by fractionation. AAPG suites, however, have higher Nb content (~10–400 ppm) and are derived from limited crust-enriched mantle interaction. Each of the IA, Syn, and NHSG suites have discrete granite subsuites distinguished using zircon morphology and geochemistry whose U-Pb ages in each case form three groups. The IA subgroups are ~867, ~847, and ~829 Ma; the Syn subgroups are ~730, 716, and 696 Ma; and the NHSG subgroups are ~636, ~610, and ~594 Ma. This apparent subevent repetition suggests some form of magmatic pulsing in the Arabian Shield. It is suggested that IA+Syn suites reflect typical volcanic arc granite settings and incremental subduction/accretion of eastward-migrating oceanic fragments of the East African Orogen. The appearance of ~636 Ma A-type magmatism within suture zones (NHSG) is possibly derived from a long-lived (~50 m.yr.) melting, assimilation, storage, and homogenization (MASH) zone resulting from an ~640 Ma slab tear. These A-types are distinguished from more-enriched anorogenic (<600 Ma) A-types, possibly associated with lithospheric delamination.

Online enhancements: appendixes.

Introduction

Given its capacity to preserve a geochronological, isotopic, and coherent trace element record of the magmas from which it crystallized, zircon is increasingly used as a petrogenetic tool (e.g., Hoskin and Schaltegger 2003; Belousova et al. 2006; Grimes et al. 2009). The Arabian-Nubian Shield (ANS) is an amalgamated collage of juvenile early Neoproterozoic to Cambrian volcanic arcs and back-arc basins (Johnson et al. 2011), and throughout and directly following this accretionary history the ANS was intruded by voluminous granites whose diverse geochemical compositions record the tectonically controlled changes in magmatic sources and processes. The systematic change in ANS tectonic processes provides the ideal opportunity to use zircon geochemistry to further constrain existing whole-rock-based models. Prior studies have argued that systematic changes in granite chemistry in part reflect changes in a mantle component of the granite magmas from depleted mid-ocean ridge basalt (MORB)–like to enriched (Stein and Goldstein 1996; Stoeser and Frost 2006; Be′eri-Shlevin et al. 2010). Focusing on A-type granites (Frost et al. 2011), which are commonly associated with fractional crystallization of magmas produced during crustal extension (Turner et al. 1992), recent ANS studies in Sinai suggest that two distinct mantle sources are involved in the tran-

Manuscript received May 10, 2015; accepted July 14, 2015; electronically published October 8, 2015.

* Author for correspondence; e-mail: frobinson685@gmail.com.

[The Journal of Geology, 2015, volume 123, p. 463–489] 0022-1376/2015/12305-0004$15.00. DOI:10.1086/683192

sition from postcollisional/calcalkaline to anorogenic alkaline granitoids (Eyal et al. 2010; Azer and Farahat 2011). This apparent source transition combined with a trend toward very voluminous, widespread magmatism following supercontinental amalgamation is often attributed to the impact of slab rollback/tear (Gvirtzman and Nur 1999; Flowerdew et al. 2013) and/or to lithospheric delamination (Avigad and Gvirtzman 2009). Alternatively, Stein and Goldstein (1996) also proposed the impact of an enriched mantle plume (with or without crustal overprinting).

To examine the systematic changes in ANS granite sources, this work focuses on the Saudi Arabian part of the ANS. Zircon geochemical data are presented from the four discrete granite evolution stages outlined by Robinson et al. (2014): (1) the island arc stage (~845 Ma), (2) the synorogenic stage (~715–700 Ma), (3) the postorogenic stage (~640–600 Ma), and (4) the late anorogenic stage (<600 Ma). The zircon geochemistry in this study is linked with prior whole-rock data from Robinson et al. (2015) with the aim of identifying trace element discriminators that support the progressive changes in granitic sources during the accretion and cratonization of the ANS. An additional tool used in this study is provided by the morphology of zircon. Prior work (e.g., Pupin 1980; Belousova et al. 2006) has shown a systematic response in zircon crystal morphology both to temperature of crystallization and to magma chemistry. The zircon morphology from island arc, synorogenic, and postorogenic granites in this study are coupled to U-Pb data from Robinson et al. (2014), which led to identification of discrete ages in this study. These discrete ages are used in a fashion similar to that in Gagnevin et al. (2011) and Schaltegger et al. (2002) to infer magmatic pulsing from lower crustal sources, which are quite distinct from the anorogenic A-types associated with an enriched, limited crust-mantle source.

Arabian Shield Geologic Setting

The Arabian Shield forms a series of tectonostratigraphic terranes composed of geochemically diverse early Neoproterozoic to Cambrian (~850–525 Ma) granitoids intruding volcanosedimentary basin assemblages. With a general younging toward the east (Stoeser and Camp 1985; Stoeser and Frost 2006; Johnson et al. 2011), the Arabian Shield is composed of eight discrete terranes separated by five ophiolite-bearing suture zones. The Arabian Shield structure consists of two parts: the western side, comprising the Midyan, Hijaz, Jiddah, and Asir island arc terranes, and the eastern side, comprising the Tathlith, Ha'il, Afif (including Khida subterrane), Ad Dawadimi, and Ar Ryan terranes (fig. 1). According to Johnson et al. (2011), these terranes have been deformed by at least four periods of arc collision and suturing and are overlain and intruded by postamalgamation (<640 Ma) basins (e.g., Nettle et al. 2014) and granitoids. The amalgamated terranes have been affected by multiple exhumation and erosion events. A Cambrian regional unconformity postdates the youngest plutons, recently dated at ~525 Ma (Robinson et al. 2014).

The Arabian Shield preserves a series of discrete Neoproterozoic tectonomagmatic events initially defined and described by Bentor (1985) and later by Stein and Goldstein (1996). In general, the earliest (~950–650 Ma) oceanic tholeiite and bimodal volcanism is confined to the western Arabian Shield, has island arc chemistry, and is emplaced in intraoceanic settings. The younger phases that intrude large areas of the western and eastern Arabian Shield and are dominated by ~640–590 Ma calcalkaline batholiths terminating at a stage of regional exhumation coupled with a switch to ~590–550 Ma alkaline granites and volcanics (Black and Liegeois 1993). The ~780–600 Ma collision of the Yanbu and B'ir Umq Sutures in the west and of the Nabitah and Halaban Sutures in the east resulted in extensive north-south-trending granitoid intrusions derived from subduction and back-arc environments. The north-south-trending Nabitah Suture forms the most significant part of this magmatic history and is interpreted to result from collision between western island arcs and the eastern partly continental Afif terrane, with proposed pre-Neoproterozoic continental crust (Stoeser and Camp 1985; Stoeser and Frost 2006). This suture consists of deformed volcanics/precollision basins intruded by postcollision granitoids/basins, and according to Johnson et al. (2011) the diachronous Nabitah Suture initiated at ~680 Ma in the north (Midyan, Hijaz, and Afif terranes) while subduction continued in the south (Asir, Tathlith, and Afif terranes). Recent studies conducted by Flowerdew et al. (2013) demonstrated that the Nabitah Suture south of the Ruwah fault zone separates juvenile Neoproterozoic intraoceanic arc terranes and propose that plutons confined to its southern end form as a consequence of subduction slab rollback. It is speculated that the terranes on either side of the Nabitah Suture were amalgamated by ~640 Ma but that farther east in the Ar Ryan and Ad Dawadimi terranes subduction and terrane assembly continued until after ~600 Ma (Doebrich et al. 2007; Cox et al. 2012).

Recent Arabian Shield geochronological data from Robinson et al. (2014) distinguished island arc (845 Ma), synorogenic (~715–710 Ma), postorogenic (~640–600 Ma), and anorogenic (<600 Ma) magmatism

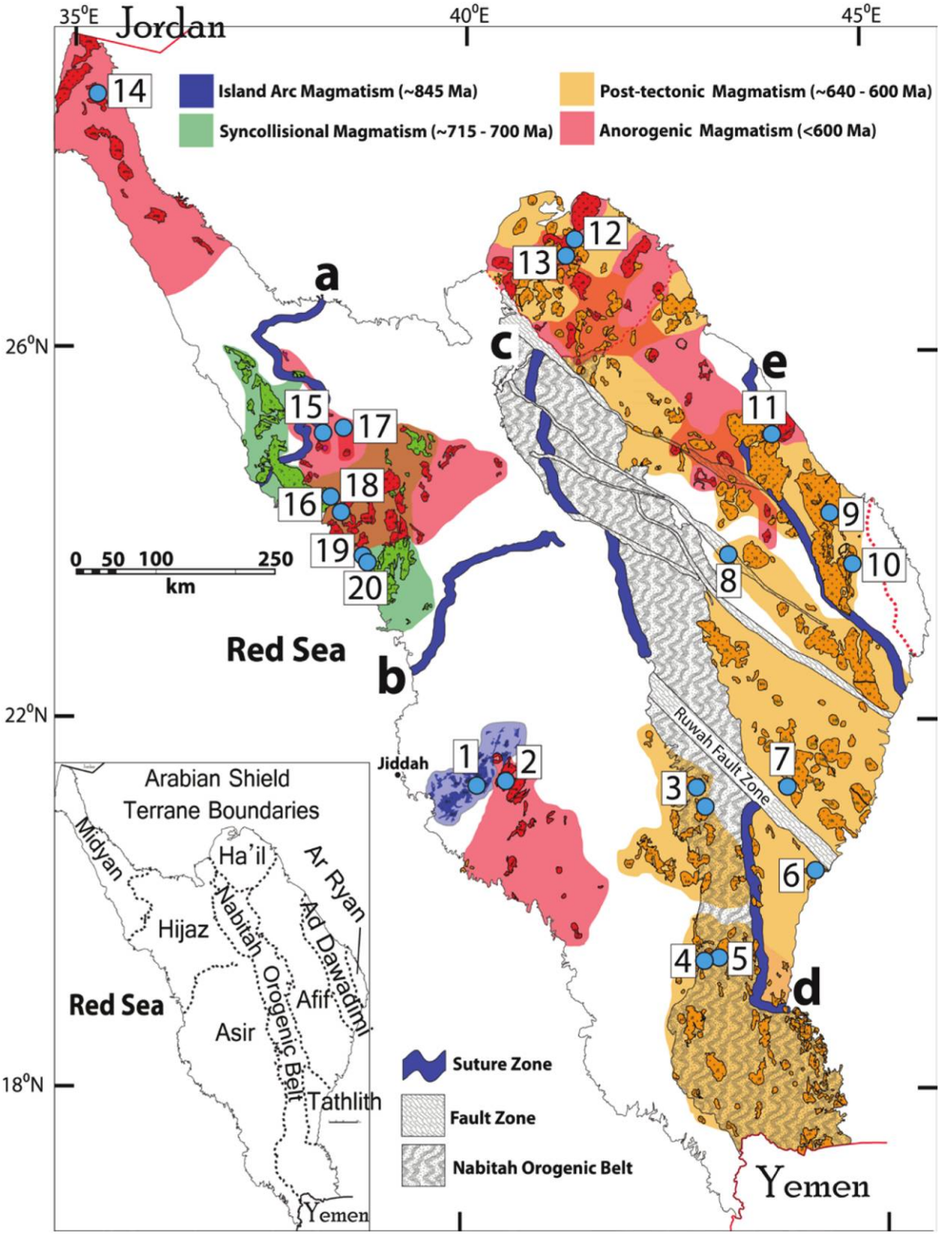

Figure 1. Geologic map of the Arabian Shield from Robinson et al. (2014) highlighting 20 sampled suites (blue circles) and their respective tectonic timing. Sample location numbers corresponding to suite names are presented in table 1. a = Yanbu Suture (~715 Ma collision of Midyan-Hijaz terranes); b = B'ir Umq Suture (~780–680 Ma collision of Hijaz-Asir terranes); c = Nabitah Suture (~680–640 Ma collision of Hijaz-Afif terranes); d = Nabitah Suture (~680–640 Ma collision of Asir-Afif terranes); e = Halaban Suture (~700–600 Ma collision of Afif-Ad Dawadimi plus Ar Ryan terranes).

(fig. 1). These cycles represent different tectonic processes in Arabian Shield evolution and produced a diverse range in granitoid mineralogy. According to recent whole-rock geochemical classification by Robinson et al. (2015), the island arc and synorogenic phases are I-type granitoids that are generated in subduction settings from MORB-like or arc tholeiite–like mafic parents. The postorogenic magmatism that appears at the termination of orogenic sutures (e.g., Nabitah Suture) is also classified as I-type. However, these suites also include aegirine-bearing A-type granites. As suggested by Robinson et al. (2015), the postorogenic granites are generated from contaminated island arc tholeiite (IAT) and MORB-like basic magmas in lower crustal zones followed by fractionation. Anorogenic suites are also A-type granites, but they are derived from a distinct heavy rare earth element (HREE)–enriched source and are interpreted to be emplaced in back-arc settings and associated with lithospheric delamination. Taking this diversity into account, this study will maintain the island arc, synorogenic, postorogenic, and anorogenic phases defined by Robinson et al. (2014) and use these as a systematic way to present the zircon geochemistry from 19 samples and support the tectonic models discussed in Robinson et al. (2015). The geochronological and geochemical properties of these samples are summarized in table 1.

Analytical Techniques

Standard reference geochemistry is presented in appendix A, tables A1–A19 (apps. A–D are available online).

Zircon Geochemistry. Following U-Pb geochronology and Hf isotopic investigation in Robinson et al. (2014), 273 zircons from 19 samples were ablated for geochemical analysis. Zircon grains were selected on the basis of (*a*) the availability/size of zircon surface area, (*b*) compositional zoning, and (*c*) concordancy. Zircons were typically >100 μm, yielded >90% concordant U-Pb ages, and were ablated using a beam diameter of 75 μm and a frequency of 5 Hz. Laser ablation inductively coupled plasma mass spectrometry (LA-ICPMS) analysis was performed using an Agilent 7500cs ICPMS coupled with a New Wave 213-nm Nd-YAG laser at Adelaide Microscopy. Ablation and machine isotope fractionation were corrected using the internationally recognized National Institute of Standards (NIST) 610 standard (element concentration: 450 ppm [±2%–5%]; Norman et al. 1996), and internal accuracy was checked using the NIST 612 standard (element concentration: 35 ppm [±2%–5%]; Norman et al. 1996). NIST 610 and NIST 612 yielded average trace element concentrations of ~440 ± 16 ppm (1 SD; n = 160) and ~34 ± 2 ppm (1 SD; n = 50), respectively.

Si^{29} was used as the calibration standard for both the NIST glasses and unknown zircon analyses. All unknown zircon grains were assigned the value of 31.57 SiO_2% (zircon mineral formula: $ZrSiO_4$ [SiO_2 = 31.57% and ZrO_2 = 58.27%]), which is assumed to be homogenous across all grains. The error associated with any SiO_2 variation—hence, unknown trace element data—is considered to be within the error range of 2%–5%, correlating with NIST 610 and 612 values. Na^{23}, Mg^{24}, Al^{27}, P^{31}, K^{39}, Ca^{43}, Ti^{43}, and Fe^{57} were used as a monitor for accidental mineral inclusion ablation (e.g., apatite). Some analyses contained >10,000-ppm P^{31} and Ca^{43} with many HREE values in the thousands of parts per million (indicative of apatite); as a result, they were discarded. This was also reflected in the isotopic signal, which displayed sharp peaks and/or troughs disrupting a stable signal. Only stable isotope signals were used in this study, which typically produced REE concentrations ranging from 1 to 5000 ppm. This range was also recorded within a single sample depending on the zircon morphology and zonation characteristics. Stable isotope signals were selected and processed using GLITTER software (Griffin et al. 2008).

Results

Zircon trace elements are summarized in table 2, and the raw data are presented in appendix A, tables A1–A19. The corresponding cathodoluminescence images are displayed in appendix B, figures B1–B19.

Zircon Geochemistry. Island arc and synorogenic (IA+Syn) zircons have a large range in Al (1.3–6235 ppm), Mg (2.1–3919 ppm), P (252–4651 ppm), Ti (3.9–917 ppm), and Fe (18–8032 ppm), and the highest values are the highest of any suite sampled. They also have among the highest Na (7.5–1906 ppm), K (2.7–1119 ppm), and Ca (84–15,985 ppm) concentrations. The lowest and highest values correlate to the synorogenic Jar-Salajah Complex with the exception of Fe, Na, Ca, and P, which correspond to the island arc Makkah Suite. IA+Syn zircons also possess the lowest values of Hf (5298–12,305 ppm), Nb (0.7–10.1 ppm), U (31–1004 ppm), light rare earth elements (LREEs; 6–1301 ppm), and HREEs (1149–10,274 ppm) of any suite sampled. The lowest values correlate with the Makkah Suite, while the highest values (excepting Zr and Hf) correlate with the Jar-Salajah Complex. As illustrated in figure 2, IA+Syn zircons form data clusters that are ~10 times lower in element concentration than other groups. The IA+Syn zircons are the most primitive in all elements,

Table 1. Summary of Sampled Plutons from the Arabian Shield

Shield terrane	Geologic map unit	Latitude	Longitude	Fig. 1 location no.	Rock type	U-Pb age (Ma)	Tectonic timing	I-S or A-type	Fe or Mg	Setting
Asir	Makkah Suite (dm)	21°21′36.45″N	40°15′44.86″E	1	Gabbro/tonalite	845.6	Island arc	I	M	VAG
Hijaz	Shufayyah Complex (su)	23°44′42.76″N	38°46′50.11″E	20	Granodiorite/ tonalite	715.4	Synorogenic	I	M	VAG
Hijaz	Jar-Salajah Complex (js)	24°24′37.62″N	38°21′23.72″E	16	Granodiorite	709.5	Synorogenic	I	M	VAG
Hijaz	Subh Suite (sf)	23°45′39.13″N	38°45′09.74″E	19	Rhyolite	698.7	Synorogenic	...	...	...
Tathlith	Al Hafoor Suite (ao)	20°23′40.32″N	44°18′05.19″E	6	Alkali granite	636	Postorogenic	I and A	F and M	VAG
Asir	Ibn Hashbal Suite (ih)	19°29′13.91″N	42°59′44.39″E	5	Alkali granite	617.6	Postorogenic	A	F and M	VAG
Asir	Wadbah Suite (wb)	19°27′09.68″N	42°49′58.70″E	4	Alkali granite	615.9	Postorogenic	A	F	WPG
Ad Dawadimi	Ar Ruwaydah Suite (ku)	24°22′43.75″N	44°21′40.56″E	9	Granite	611	Postorogenic	A	F	WPG
Asir	Kawr Suite (kw)	21°20′10.17″N	42°45′05.29″E	3	Alkali granite	611.7 and 608	Postorogenic	I and A	F and M	VAG/ WPG
Afif	Haml Suite (hla)	21°18′13.29″N	43°51′21.78″E	7	Quartz-monzonite	608.6	Postorogenic	Borderline I and A	M	VAG
Ad Dawadimi	Najirah Granite (nr)	23°43′43.93″N	44°41′21.06″E	10	Granite/alkali granite	607	Postorogenic	A	F	WPG
Ha′il	Idah Suite (id)	27°03′44.28″N	41°17′58.70″E	13	Alkali granite	605.8	Postorogenic	Borderline I and A	F	VAG
Afif	Al Khushaymiyah Suite (ky)	23°49′39.69″N	43°11′42.07″E	8	Quartz-monzonite	601.2	Postorogenic	Borderline I and A	M	VAG
Hijaz	Rithmah Complex (rt)	25°09′07.90″N	38°11′20.41″E	15	Diorite/gabbro	600	Anorogenic	...	...	...
Ad Dawadimi	Malik Granite (kg)	25°07′56.42″N	43°47′10.82″E	11	Leucogranite	599.4	Anorogenic	S	F and M	VAG
Hijaz	Admar Suite (ad)	24°17′53.09″N	38°24′43.55″E	18	Syenite	599.2	Anorogenic	Borderline I and A	M	VAG
Midyan	Al Bad Granite Super Suite (abg)	28°44′32.20″N	35°20′12.32″E	14	Alkali granite	597.4	Anorogenic	A	F and M	WPG
Asir	Al Hawiyah Suite (hwg)	21°26′54.04″N	40°27′16.45″E	2	Granite	591.9	Anorogenic	A	F	WPG
Ha′il	Abanat Suite (aa)	27°18′43.63″N	41°24′33.52″E	12	Alkali granite	585	Anorogenic	A	F	WPG
Hijaz	Mardabah Complex (mr)	25°11′29.42″N	38°29′35.33″E	17	Syenite	525.6	Anorogenic	A	F	WPG

Note. Zircon U-Pb ages are from Robinson et al. (2014), while whole-rock geochemical granitoid classifications are from Robinson et al. (2015). VAG = volcanic arc granite; WPG = within-plate granite; F = ferroan; M = magnessian.

Table 2. Summary of Zircon Laser Ablation Inductively Coupled Plasma Mass Spectrometry Trace Element Data Obtained from 18 Dated Suites across the Arabian Shield

	Island arc (~845 Ma)			Synorogenic (~715–700 Ma)							Postorogenic (~640–600 Ma)					
	Makkah Suite, dm01a			Jar-Salajah Complex, js202			Shufayyah Complex, su216			Subh Suite, sf209	Al Hafoor Suite, ao85	Kawr Suite, kw42			Kawr Suite, kw51p	Ibn Hashbal Suite, ih68
	MC1	MC2	MC3	MC1	MC2	MC3	MC1	MC2	MC3			MC1	MC2	MC3		
Na23	1384.6	1181.0	1447.0	193.8	177.2	81.8	79.5	101.2	101.6	144.7	125.5	139.3	188.2	306.4	197.5	22.4
Mg24	254.8	114.7	68.5	38.3	1067.4	135.2	31.7	99.4	212.9	32.7	21.7	71.0	326.2	805.4	102.6	29.6
Al27	324.8	300.7	140.6	310.3	1878.3	422.4	103.7	323.3	422.9	209.0	184.6	227.1	509.0	880.4	828.7	147.9
P31	2516.3	1501.9	2665.9	441.0	1202.2	438.9	523.1	443.9	512.0	542.4	637.5	563.5	652.4	776.2	337.7	353.6
K39	139.1	136.6	173.6	237.2	720.5	217.9	23.3	118.8	49.9	162.4	55.8	96.6	155.9	124.7	134.8	24.4
Ca43	9174.4	10,244.1	9835.7	819.8	2225.4	426.4	813.2	738.5	1025.7	802.2	1510.8	1386.5	1729.1	1775.2	1357.9	556.9
Ti49	51.3	31.2	33.5	16.8	268.2	189.9	13.1	42.2	147.6	60.9	14.9	18.9	29.2	34.7	41.5	20.3
Fe57	808.3	487.6	260.2	432.2	2412.9	683.8	207.6	628.1	721.4	387.2	477.2	282.2	757.4	1516.7	1031.2	810.7
Rb85	.3	.4	.3	.6	4.0	1.0	.2	.4	.3	.5	.3	.7	.5	.6	1.0	.3
Sr88	.3	1.0	.2	.9	8.3	1.1	1.4	1.6	4.5	1.0	5.7	3.3	7.0	11.4	14.1	2.4
Y89	1787.4	1296.9	1118.7	3371.3	4675.2	1910.0	1771.8	2316.4	2488.4	3639.1	1882.0	2167.1	2622.2	2696.3	2857.6	3118.1
Nb93	2.1	1.7	1.5	2.0	5.0	2.3	1.6	1.4	3.3	2.6	4.7	7.3	10.3	12.2	89.7	24.7
La139	.0	.1	.0	1.8	24.2	1.8	1.4	.8	2.6	2.4	18.1	11.9	43.6	39.3	25.5	62.0
Ce140	35.3	27.6	23.3	12.4	168.3	18.5	22.8	21.8	81.6	16.5	78.0	65.8	140.8	171.1	161.6	189.0
Pr141	.2	.3	.2	.9	20.5	1.2	.8	.5	2.2	1.2	9.6	6.9	18.0	24.3	25.1	19.2
Nd146	4.0	3.8	3.2	9.7	131.9	8.4	6.4	5.3	17.2	11.5	51.6	42.7	102.1	133.7	155.3	115.7
Sm147	7.1	5.7	5.5	21.4	78.2	8.6	6.6	8.1	11.9	21.6	33.9	32.9	59.7	64.4	110.9	63.4
Eu153	3.7	2.9	2.8	13.5	6.1	.9	1.2	1.4	1.7	9.3	1.4	1.7	1.8	1.7	4.2	4.3
Gd157	33.8	24.4	24.1	110.5	180.7	36.7	32.9	44.0	45.2	108.9	65.8	82.4	116.5	112.5	175.6	154.5
Tb159	12.0	8.7	8.5	36.5	50.8	13.5	12.0	16.2	16.3	36.5	19.3	26.2	38.6	33.8	48.9	43.4
Dy163	152.3	107.9	101.6	375.9	513.6	169.9	153.0	205.8	206.3	391.2	196.4	269.1	384.2	335.2	428.0	413.7
Ho165	60.8	43.5	39.2	123.9	166.9	67.0	60.2	81.0	82.9	133.8	66.5	85.4	112.5	103.8	116.1	123.6
Er166	293.1	214.2	185.7	501.8	675.0	307.8	277.7	366.8	391.1	549.1	286.8	333.3	426.8	421.3	427.4	442.0
Tm169	75.9	56.9	48.1	102.9	138.3	70.3	64.0	82.1	89.3	113.4	67.9	72.4	90.3	93.2	88.6	79.9
Yb172	900.2	684.9	571.6	959.1	1272.7	700.6	649.9	796.7	887.8	1045.2	731.3	713.7	859.1	928.8	820.4	648.2
Lu175	151.6	116.6	95.5	158.6	219.3	126.3	112.5	143.8	167.1	174.5	110.4	98.2	122.6	139.3	109.0	93.4
Hf178	7271.2	7078.0	8324.4	8532.6	9382.0	10,183.6	9223.7	10,069.0	11,016.6	9173.1	11,317.0	9524.5	11,016.6	12,726.1	13,414.6	7528.1
Pb208	18.7	13.0	11.1	5.4	13.6	4.7	4.6	9.3	10.8	6.4	40.1	25.7	27.1	43.6	72.8	13.6
Th232	233.2	163.1	142.7	71.8	323.3	77.7	68.3	131.3	233.5	99.6	578.8	389.8	400.2	590.7	622.5	237.7
U238	277.9	200.2	166.1	212.3	520.1	230.5	212.9	282.3	614.5	266.0	1701.9	1287.8	1143.9	2006.1	1798.3	696.2
No. zircons	4	8	5	6	4	9	4	7	4	10	11	8	12	6	11	15

	Postorogenic (~640–600 Ma)										Anorogenic (<600 Ma)				
	Najirah Granite, nr120			Wadbah Suite, wb65			Haml Suite, hla110	Ar Ruwaydah Suite, ku139	Idah Suite, id159	Al Khushaymiyah Suite (ky)	Admar Suite, ad194	Malik Granite, kg150	Al Bad Suite, abg179	Al Hawiyah Suite (hwg)	Mardabah Complex, mr191
	MC1	MC2	MC3	MC1	MC2	MC3									
Na23	13.8	20.4	116.2	19.8	21.8	15.4	43.8	1311.3	181.8	31.9	6.7	68.6	235.3	184.2	1540.8
Mg24	3.8	105.0	282.7	3.1	11.5	52.7	85.1	93.3	101.6	98.0	5.8	61.1	385.0	247.4	54.2
Al27	38.3	534.5	927.8	11.5	128.3	107.5	214.3	785.1	748.5	302.8	25.7	208.4	1367.7	1021.1	106.4
P31	320.9	489.1	615.6	264.7	583.4	165.7	1275.4	983.4	1350.3	292.3	184.5	398.9	1032.8	522.9	1545.1
K39	7.4	47.6	38.6	12.6	39.6	10.2	38.6	273.5	172.8	26.5	4.9	118.1	268.7	218.4	148.7
Ca43	366.6	737.2	1020.6	391.2	1477.3	166.1	3366.6	8251.7	5331.4	325.6	116.3	561.2	1340.9	1386.5	10,755.5
Ti49	9.9	21.9	31.8	11.2	17.6	11.6	22.1	44.9	52.5	19.6	18.2	14.5	45.1	30.0	61.8
Fe57	255.6	423.5	588.0	125.6	702.4	695.8	400.6	1563.6	2735.2	742.2	345.6	277.1	943.1	658.6	733.8
Rb85	.3	.8	.8	.1	.4	.2	.3	.8	1.3	.3	.1	1.0	2.3	2.1	.3
Sr88	.8	4.1	10.4	.3	1.0	.5	3.3	101.9	30.2	2.1	.3	2.3	24.1	12.6	1.9
Y89	1450.9	2768.9	3747.7	1181.0	1362.8	1406.5	824.6	2499.5	3426.9	1674.2	641.1	3295.1	5570.3	3155.1	1439.9
Nb93	2.6	12.0	23.2	3.8	4.2	4.6	2.5	9.2	70.9	3.1	.9	21.8	43.0	172.6	12.5
La139	2.3	10.1	16.7	6.2	12.5	.7	25.7	130.0	169.9	18.0	.7	20.2	111.9	28.3	.7
Ce140	12.5	50.8	122.9	30.8	46.1	22.6	96.1	527.0	296.1	135.0	41.4	134.2	1675.3	115.0	18.6
Pr141	1.4	6.2	12.3	3.0	6.1	1.1	12.7	71.2	36.4	5.8	.4	10.1	54.6	14.6	.4
Nd146	12.6	39.9	77.2	20.9	40.6	12.5	71.9	467.1	182.7	29.2	5.4	63.8	263.5	81.2	5.3
Sm147	10.7	30.4	54.5	15.7	25.7	16.3	25.5	185.5	90.0	13.7	7.4	42.4	145.5	39.4	8.6
Eu153	.9	2.2	6.4	1.8	9.2	3.9	1.7	11.8	3.7	5.1	2.0	2.8	6.9	7.0	1.2
Gd157	41.8	94.2	139.0	50.8	66.7	57.6	32.6	190.3	155.4	51.9	26.2	127.3	246.9	85.0	38.6
Tb159	13.9	30.7	44.1	14.5	18.5	16.7	7.9	31.8	45.3	15.9	7.2	39.7	67.0	28.9	13.1
Dy163	154.5	319.3	444.4	145.5	177.9	168.8	80.0	270.2	427.8	174.3	71.7	407.5	637.7	322.9	146.0
Ho165	53.5	102.0	138.0	46.2	53.7	54.3	28.2	86.3	125.5	60.1	23.3	128.7	203.8	110.6	49.5
Er166	217.6	395.4	532.2	175.0	199.1	206.6	124.6	354.5	483.3	251.6	92.7	490.7	832.7	473.4	197.2
Tm169	44.9	78.6	106.3	35.9	40.1	42.2	29.3	78.9	103.8	58.3	18.8	97.5	180.3	106.8	40.7
Yb172	420.5	699.9	954.0	338.1	373.4	391.8	310.0	811.1	997.9	618.8	175.4	873.7	1724.1	1072.9	372.5
Lu175	65.6	105.4	144.2	49.3	55.4	57.4	49.2	123.2	141.5	89.0	31.1	129.7	275.4	153.5	51.7
Hf178	9802.8	10,496.1	11,715.1	9062.9	8597.5	9948.9	10,347.5	11,182.6	10,222.8	8711.6	7726.1	10,833.8	11,509.5	12,036.6	8118.5
Pb208	2.5	9.9	16.3	2.3	19.2	4.9	10.6	115.2	33.5	45.5	2.5	13.6	65.9	67.8	10.0
Th232	44.7	114.9	173.9	39.8	46.4	57.3	168.3	1144.7	471.3	826.6	46.2	252.7	768.9	371.7	150.3
U238	147.0	484.0	897.6	160.9	169.8	237.8	452.0	4743.5	991.6	721.9	54.4	683.0	995.2	1424.9	248.2
No. zircons	4	11	9	4	8	4	11	15	12	7	19	5	12	14	14

Note. All 273 zircon analyses and corresponding cathodoluminescence images are displayed in appendixes A and B, respectively. Values were processed using GLITTER software (Griffin et al. 2008). MC designates the zircon morphological classes within a given suite.

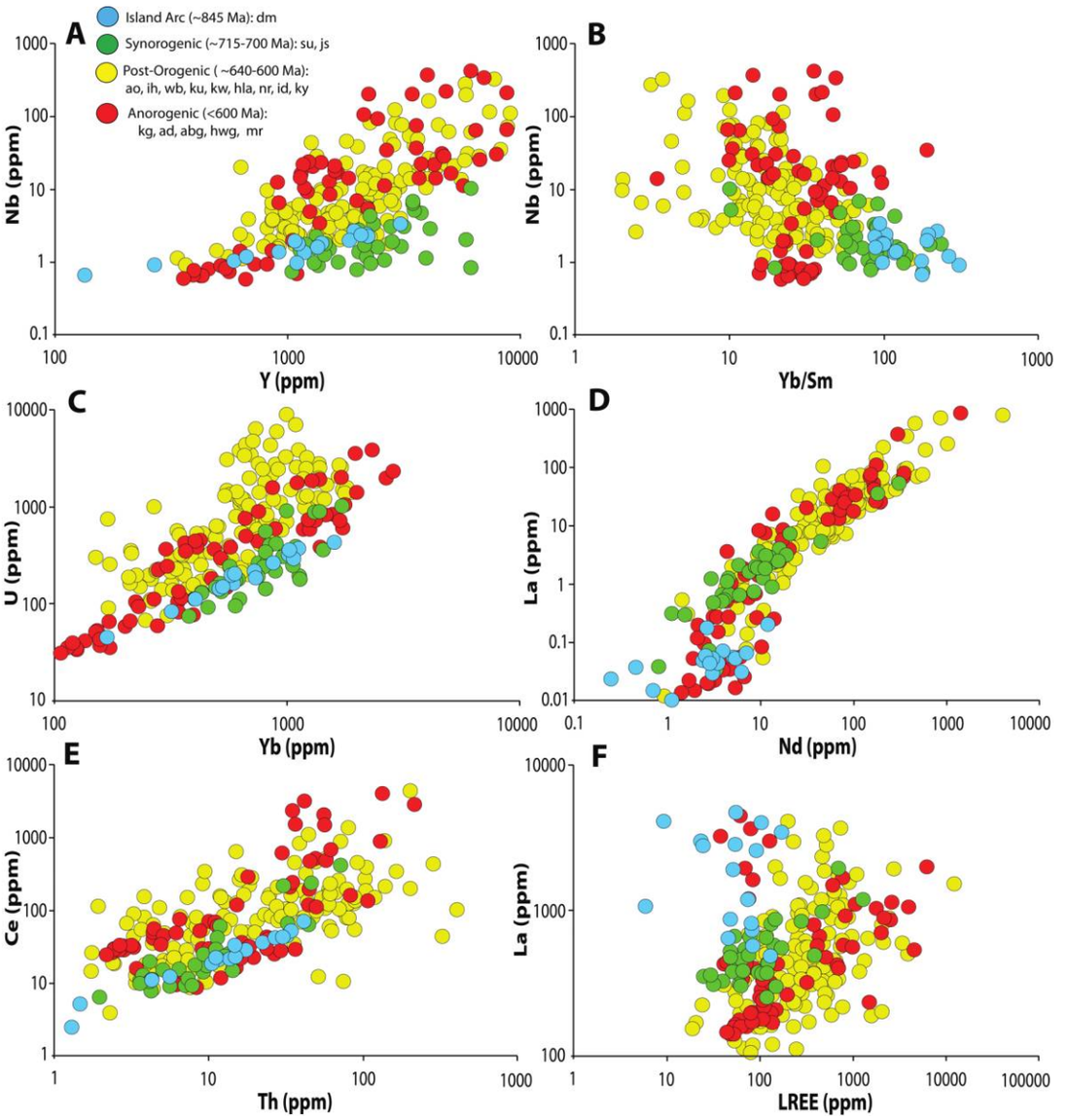

Figure 2. Selected zircon trace element plots for the four age groups sampled in the Arabian Shield. Arabian suite abbreviations are presented in table 1.

but IA zircons contain among the highest La concentrations (fig. 2). IA+Syn trace element signatures exhibit a positive HREE enrichment gradient but a depletion in LREE and HREE concentrations compared with other groups (fig. 3). This is particularly noted with IA zircons, which also display strong negative La, Pr, Sr, and Nd anomalies and a positive Ce anomaly. Synorogenic signatures are ~10-fold more enriched in LREEs than in IA zircons and also contain similar La, Pr, Sr, and Ce anomalies. However, synorogenic zircons contain negative K and Eu anomalies (fig. 3), indicative of feldspar fractionation.

Postorogenic suites have a large range in Na (3.4–2290 ppm), Mg (0.2–2733 ppm), Al (3.4–2729 ppm), P (105–4061 ppm), Ca (77–23,514 ppm), K (2.3–998 ppm), Ti (4.1–269 ppm), Fe (25–6705 ppm), Hf (7218–15,772 ppm), Nb (1.1–317 ppm), U (67–11,458 ppm), LREEs (21–3983 ppm), and HREEs (619–14,136 ppm), in which the highest values are similar to anorogenic abundances and are among the highest of sampled suites. The lowest and highest values correspond to the Kawr Suite and the Ar Ruwaydah Suite, respectively. Postorogenic zircon geochemistry shows extensive mingling with

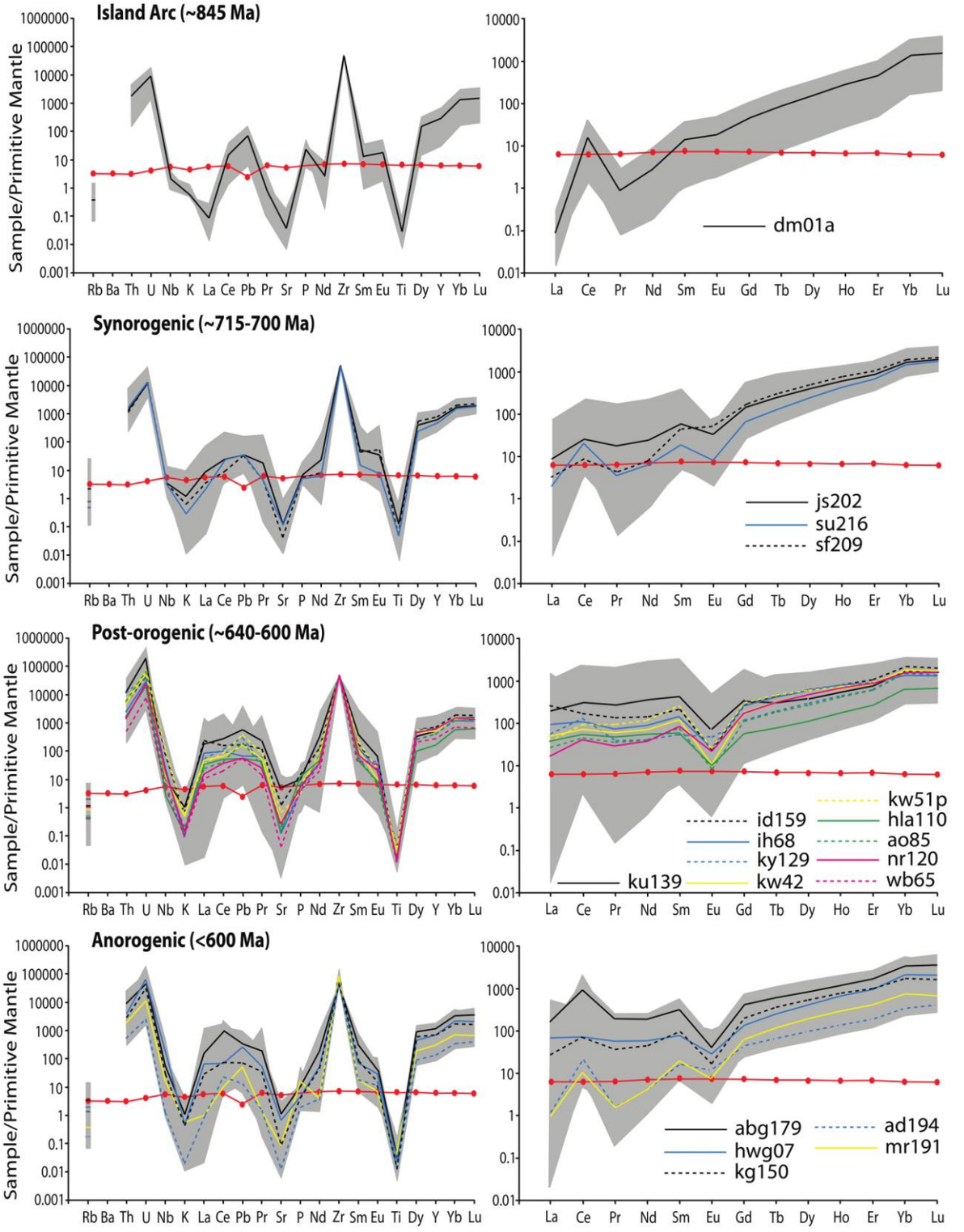

Figure 3. Primitive mantle normalized rare earth element patterns of sampled Saudi Arabian zircons. The gray field is the tectonic group composition range, and the solid and dashed lines are the average values for each sampled suite. The red line is the average midocean ridge basalt composition from Jenner and O'Neil (2012). Samples were normalized to primitive mantle values from Sun and McDonough (1989).

anorogenic suites, and alongside anorogenic suites they form distinct groups isolated from older IA+Syn zircons (fig. 2). This is particularly notable with Nb, U, and La. Postorogenic suites have the most diverse trace element signatures of all magmatic age groups and exhibit a large composition range with both LREE and HREE enrichment (fig. 3). The LREE signatures are ~100 times greater than the older IA+Syn suites and are marginally higher than anorogenic suites, making these the most enriched of all magmatic suites. These have distinctive negative K, Sr, and Eu depletions indicative of feldspar fractionation, but they are absent of La, Pr, and Ce anomalies present in similar anorogenic A-type suites (fig. 3). However, postorogenic suites have half an order of magnitude greater in middle REE abundances.

Anorogenic zircons have the lowest and highest concentration of K (2.4–1167 ppm) of any suite sampled in the Arabian Shield. Similarly, Na (3.4–2312 ppm), Ca (71.4–21,102 ppm), Al (2.5–3342 ppm), Mg (0.2–1068 ppm), P (69–4406 ppm), Ti (4.3–224 ppm), and Fe (31–5353 ppm) concentrations are also among the lowest and highest. In general, the Al Bad Suite correlates with the highest values, while the Admar Suite syenite corresponds with the lowest values. Trace element values also have a large range and include Hf (4746–15,090 ppm), Nb (0.6–411 ppm), LREEs (41–6361 ppm), and HREEs (602–15,258 ppm), with the highest concentrations the highest of any suite sampled in the Arabian Shield. The majority of lowest and highest REE values correlate with the Admar Suite and the Al Bad Suite, respectively. As illustrated in figure 2, anorogenic trace elements have values similar to those of postorogenic suites. These age groups both have A-type whole-rock geochemistry (Robinson et al. 2015) and unsurprisingly show extensive mingling with zircon geochemistry. Most importantly, the most evolved anorogenic geochemistry is consistently separated from older IA+Syn zircons (fig. 2). However, when utilizing La, Nb, and Ce, the primitive Admar Suite syenite shows some mingling with the island arc geochemistry. Anorogenic trace element signatures exhibit both LREE and HREE enrichment, and the LREE abundances are ~100 times greater than those in older IA+Syn suites (fig. 3). Similarly, they also have strong negative La, Pr, Sr, and Eu anomalies indicative of feldspar fractionation. Although anorogenic signatures are similar to those of postorogenic suites, they are lower in LREEs and possess distinctive positive Ce and negative Pr anomalies (fig. 3).

Distinguished Zircon Morphology. Zircon morphologies were differentiated by Cl imagery, following the work of Pupin (1980), and discrete morphological subgroups were defined in the island arc (Makkah Suite), synorogenic (Shufayyah Complex and Jar-Salajah Complex), and postorogenic (Kawr Suite, Najirah Granite, and Wadbah Suite) magmatic groups (table 3). These suites contain a mixture of stubby well-zoned, stubby poorly zoned, elongate well-zoned, and elongate poorly zoned morphologies that have been thoroughly described in Robinson (2014). In general, there is a trend toward the oldest I-type suites having zircon morphologies with lower temperatures (~650°–750°C) and the younger A-type suites having higher temperature morphologies (~750°–850°C). This trend is consistent with the findings of Belousova et al. (2006), who also evoke a possible petrogenetic difference between granites with low and high temperature zircon morphologies. In general, most sampled suites in Robinson et al. (2014) contain zircons that are entirely one type and/or occasionally one or two outliers but not a distinct mixture of morphology types in abundance. This section will describe the REE chemistry of the IA+Syn and postorogenic zircon morphology classes, which are referred to as MC throughout this section. The values are presented in table 2.

Zircons from the island arc Makkah Suite gabbrodiorite are divided into three morphological classes: MC1, stubby poorly zoned zircons; MC2, elongate well-zoned zircons; and MC3, elongate poorly zoned zircons (fig. 4). The lowest and highest values of Mg, Al, Ti, and Fe correlate to MC3 and MC1, respectively, while the lowest and highest values of Na, K, P, and Ca correspond to MC1 and MC3, respectively. MC1 has a higher abundance of HREEs and a lower concentration of LREEs, while MC3 contains lower HREEs and higher LREEs. Similarly, the Shufayyah Suite tonalite is divided into stubby poorly zoned (MC1), stubby well-zoned (MC2), and elongate well-zoned (MC3) zircons (fig. 4). The lowest and highest values of Na, Mg, Al, Ti, and Fe belong to MC1 and MC3, respectively, while P, K, and Ca are more ambiguous, with MC1, MC2, and MC3 containing similar concentration ranges. Interestingly, the LREE and HREE values show the opposite trend from the Makkah Suite, with the lowest and highest levels correlating to MC1 and MC3, respectively. Zircons from the Jar-Salajah Complex granodiorite are divided into stubby well-zoned (MC1), stubby poorly zoned (MC2), and elongate well-zoned (MC3) zircon morphologies (fig. 4). Similar to zircons of the Makkah Suite, these zircons have the lowest Mg, Al, Ti, and Fe values, correlating to MC1, and the lowest P, K, and Ca values, correlating to MC3. The highest values of all major elements, aside from Na, correspond to MC2. The lowest and highest concentrations of Na belong to MC3 and MC1, respectively. Jar-Salajah

Table 3. Summary of the Zircon Morphologies Found in Six Arabian Shield Granitoids

Sample	Terrane	Granite type	Zircon color	Approximate zircon length (μm)	Zircon shape	Zircon morphology after Pupin (1980)	Simple/complex zonation
Makkah Suite, dm01a	Asir	I-type	Yellow-brown	50–100	Stubby euhedral prisms	S13-S15 (~750°C), R2 (~700°C)	Complex
			Yellow	100–300	Elongate prisms	G1-P1 (~600°–650°C), P4 (~800°C)	Simple
			Yellow	200–400	Elongate prisms	P1-R1 (~650°C)	Complex
Shufayyah Complex, su216	Hijaz	I-type	Yellow	<100	Stubby euhedral pyramids	L2-L4, G2 (~650°C)	Simple
			Yellow-pink	50	Stubby euhedral pyramids	AB2-AB4 (~550°C), L2-L3-S2-S3 (~650°C)	Simple
			Colorless-brown	100–150	Elongate prisms	P1 (~650°C), S14 (~750°C)	Simple
Jar-Salajah Complex, js202	Hijaz	I-type	Brown	<100	Stubby euhedral pyramids	AB2-AB4, G3, S4 (~550°–650°C)	Complex
			Yellow	100–200	Elongate prisms	P4-S24(~800°–850°C), S12-S13 (~750°C)	Simple
			Yellow	<100	Stubby euhedral pyramids	AB2-AB4 (~550°C)	Complex
Najirah Granite, nr120	Ad Dawadimi	A-type	Yellow	<100	Stubby euhedral prisms	S8-S10 (~700°C), S13-S15 (~750°C)	Simple
			Pink	150–250	Elongate euhedral prisms	S18-S19 (~800°C), S23-S24 (~850°C)	Simple
			Colorless-yellow	100–300	Elongate euhedral prisms	P2-P4 (~700°–800°C)	Simple
Kawr Suite, kw42	Asir	A-type	Yellow	<100	Stubby euhedral prisms	S18-S19 (~800°C), J4 (~900°C)	Simple
			Brown-pink	100–200	Elongate euhedral prisms	S13-S14-P3-S17-S19-S24 (~750°–850°C)	Simple
			Colorless-yellow	100–200	Elongate prisms	P3-S19-S23-S24-P5-J4 (~750°–900°C)	Simple
Wadbah Suite, wb65	Asir	A-type	Yellow	<100	Stubby euhedral prisms	S15-R3 (~750°C), S18-S19 (~800°C)	Simple
			Yellow-pink	100–250	Elongate euhedral prisms	S15-P3 (~750°C), S19-S20-P4-R4 (~800°C)	Simple
			Colorless-brown	100–200	Elongate euhedral prisms	S14-S15-P3 (~750°C)	Simple

Note. Zircon details are discussed in Robinson (2014), and morphologies are described in Pupin (1980).

Figure 4. Representation of the three zircon morphologies and corresponding analyzed rare earth element (REE) and $^{206}Pb/^{238}U$ age data spots found in the island arc (Makkah Suite), synorogenic (Shufayyah and Jar-Salajah Complexes), and postorogenic (Najirah Granite, Kawr, and Wadbah Suites) magmatic groups. Morphology classes (MCs) and associated numbers refer to the number of zircons with similar morphology. The numbers 1 and 2 refer to the photographic scale assigned to the given suite.

zircons are defined from older suites by their large LREE array and elevated HREEs. The lowest and highest LREE and HREE abundances correlate to MC1 and MC3, respectively.

The postorogenic Kawr Suite granite has stubby well-zoned (MC1), elongate well-zoned (MC2), and elongate poorly zoned (MC3) zircon morphologies (fig. 4). The lowest and highest values of Na, Mg, Al, P, Ca, Ti, and Fe correlate to MC1 and MC3, respectively, while the highest values of K correlate to MC2. Similarly, the lowest and highest abundances of LREEs and HREEs correspond to MC1 and MC3, respectively. However, U is the exception, with MC1 correlating to the highest concentrations. The Najirah Granite is divided into stubby well-zoned (MC1), elongate well-zoned (MC2), and elongate poorly zoned (MC3) zircons (fig. 4). Interestingly, this shows patterns identical to those of the Kawr Suite. The lowest and highest values of Na, Mg, Al, P, Ca, Ti, and Fe correlate to MC1 and MC3, respectively. Once again, MC2 has the highest values of K, while the lowest correlates to MC1. Trace element abundances yield similar results, with the lowest and highest LREE and HREE values corresponding to MC1 and MC3, respectively. The Wadbah Suite alkali granite contains stubby well-zoned (MC1), elongate poorly zoned (MC2), and elongate well-zoned (MC3) zircons (fig. 4). The lowest and highest Mg and Fe abundances correlate to MC1 and MC3, respectively. Similarly, the lowest values of Al and Ti also belong to MC1, but instead MC2 corresponds with the highest values. Interestingly, Na, P, K, and Ca show the opposite trend, with the lowest abundances correlating to MC3 and the highest to MC2. Trace element concentrations display similar results, with the lowest and highest LREE and HREE values corresponding to MC2 and MC1, respectively.

The REE-analyzed zircon morphologies were compared with their respective $^{206}Pb/^{238}U$ age from Robinson et al. (2014) and appear to show age scatter consistent with the three distinct morphology classes (fig. 5). It should be noted that the *Y*-axis element concentration is independent of the *X*-axis zircon age; thus, any element illustrated will fluctuate according to concentration, but the age will remain the same. Consequently, Hf is chosen to highlight this scatter because it is a REE in abundance across all zircons. As illustrated in figure 5, there is also a trend toward increasing Hf concentration with decreasing age. This helps to reinforce the identification of three morphology groups in island arc, synorogenic, and postorogenic samples.

Discrete Crystallization Ages. The identification of three distinguished zircon morphologies and geochemistries in figure 5 appear to illustrate three geochronological groups. Following this, the spot $^{206}Pb/^{238}U$ ages are used to calculate a weighted average age for each morphology group (table 4). To investigate whether these morphological discrete ages are statistically one age or multiple ages, the Gaussian distribution component and the $^{206}Pb/^{238}U$ age for each sample are examined. The raw zircon age data and discrete ages are presented in appendix C, tables C1–C6.

Zircons from the Makkah Suite, Shufayyah Complex, and Wadbah Suite yield tight $^{206}Pb/^{238}U$ crystallization ages of 845.6 ± 4.9 Ma (MSWD: 1.6), 715.4 ± 3.6 Ma (MSWD: 1.2), and 615.9 ± 4.9 Ma (MSWD: 2.0), respectively, and suggest that all data lie in a near-Gaussian distribution and form a single age (fig. 6). However, three morphology groups yield distinct $^{206}Pb/^{238}U$ weighted means of 867.9 ± 8.5, 847 ± 5.3, and 829.2 ± 6.8 Ma (Makkah Suite); 730.9 ± 7.2, 716.7 ± 4.1, and 696.3 ± 7.1 Ma (Shufayyah Complex); and 629.8 ± 5.7, 614 ± 5.2, and 601.1 ± 6.5 Ma (Wadbah Suite), respectively; this hints that more than one age may exist in the combined data, which is unresolvable by the relatively imprecise LA-ICPMS technique. In addition, these suites illustrate a small break and skewed distribution in the data when a linearized probability plot from Isoplot software is used (Ludwig 2000), which may represent more than one age (fig. 6). Statistical studies from Melnykov and Maitra (2010) and Sambridge and Compston (1994) describe the separation of data clusters and multimodel distributions and highlight that multiple Gaussian distributions can add together to produce a single normal Gaussian distribution and/or that the data may not be Gaussian at all. It is suggested that this may be the case for the Makkah, Shufayyah, and Wadbah Suites, but it is unresolvable using LA-ICPMS.

Zircons from the Jar-Salajah Complex, the Najirah Granite, and the Kawr Suite, however, yield $^{206}Pb/^{238}U$ crystallization ages of 709.5 ± 8.4 Ma (MSWD: 3.5), 607 ± 7.9 Ma (MSWD: 2.9), and 611.7 ± 6.5 Ma (MSWD: 2.4), respectively, and their multipeaked probability plots coupled with large MSWD values suggest that these data form a non-Gaussian distribution with more than one age present in each distribution (fig. 6). Three morphology groups also yield distinct $^{206}Pb/^{238}U$ weighted means of 710 ± 5.0, 693.2 ± 7.5, and 676.5 ± 5.0 Ma (Jar-Salajah Complex); 631.4 ± 9.1, 606.5 ± 6.0, and 585.4 ± 8.8 Ma (Najirah Granite); and 636.6. ± 8.4, 609.9 ± 5.7, and 594.7 ± 7.6 Ma (Kawr Suite), respectively; this suggests that more than one age is present. Statistically, the Jar-Salajah Complex appears to have a distribution consistent with two ages,

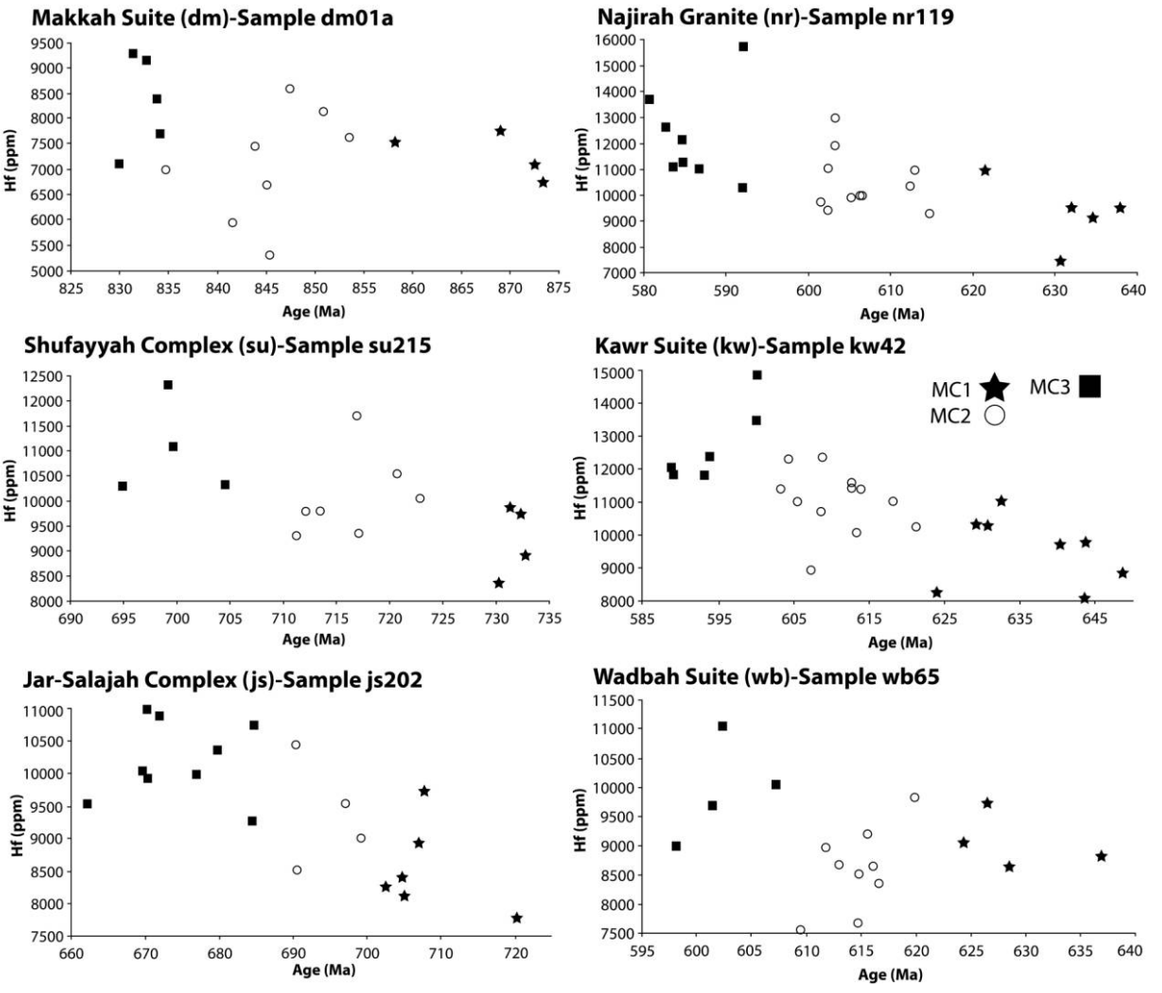

Figure 5. Identified zircon morphology classes (MCs) from island arc (Makkah Suite), synorogenic (Shufayyah and Jar-Salajah Complexes), and postorogenic (Najirah Granite, Kawr, and Wadbah Suites) magmatic groups plotted with corresponding $^{206}Pb/^{238}U$ age spots from Robinson et al. (2014).

resulting in two peaks in the probability density distribution. The Najirah Granite has three steps in the data reflecting the three discrete ages, and the Kawr Suite has a distribution suggestive of two ages (fig. 6). Once again, it is suggested that the limitations of the LA-ICPMS technique cannot resolve three discrete ages in the Jar-Salajah Complex and Kawr Suite. Overall, six samples contain three distinct age groups, and with the collection of additional U-Pb data more discrete ages could be identified, but they are not statistically supportable in this study (e.g., the Makkah Suite and the Jar-Salajah Complex have four to five steps in the data). As described in appendix D and shown in figures D1 and D2, the three discrete ages are not the product of ablation drift or Pb/Th isotope fluctuations. To help reduce Pb loss as a factor for the younger age groups, Pb, U, and Th content are plotted with age in appendix D, figures D1 and D2. Only the Jar-Salajah Complex has elevated U, which may indicate Pb loss. This is in agreement with Robinson et al. (2014).

Discussion

Zircon geochemistry data presented in this study support the four magmatic groups defined in Robinson et al. (2014): island arc (~845 Ma), synorogenic (~715–700 Ma), postorogenic (~640–600 Ma), and anorogenic (<600 Ma). Trace elements identify a distinction between older (I-type) zircons associated with subduction and younger (A-type) zircons formed in extensional environments. However, geochemical

Table 4. Sampled Granitoids Divided into Three Discrete Ages on the Basis of Zircon Morphology

Geologic unit	$^{206}Pb/^{238}U$ age (Ma)	2σ	MSWD	No. zircons	Zircon morphology	$^{206}Pb/^{238}U$ age (Ma)	2σ	MSWD	No. zircons
Makkah Suite, dmo1a	845.6	4.9	1.6	38	MC1 = Stubby poorly zoned	867.6	8.5	.27	8
					MC2 = Elongate well zoned	847.0	5.3	.29	19
					MC3 = Elongate poorly zoned	829.2	6.8	.33	11
Shufayyah Complex, su216	715.4	3.6	1.2	47	MC1 = Stubby poorly zoned	730.9	7.2	.015	9
					MC2 = Stubby well zoned	716.7	4.1	.26	29
					MC3 = Elongate well zoned	696.3	7.1	.34	9
Jar-Salajah Complex, js202	709.5	8.4	3.5	29	MC1 = Stubby well zoned	710.0	5.0	.44	12
					MC2 = Stubby poorly zoned	693.2	7.5	.28	5
					MC3 = Elongate well zoned	676.5	5.0	.60	12
Najirah Granite, nr120	607.0	7.9	2.9	20	MC1 = Stubby well zoned	631.4	9.1	.28	5
					MC2 = Elongate well zoned	606.5	6.0	.31	9
					MC3 = Elongate poorly zoned	585.4	8.8	.14	6
Kawr Suite, kw42	611.7	6.5	2.4	26	MC1 = Stubby well zoned	636.6	8.4	.49	8
					MC2 = Elongate well zoned	609.9	5.7	.23	12
					MC3 = Elongate poorly zoned	594.7	7.6	.30	6
Wadbah Suite, wb65	615.9	4.9	2.0	26	MC1 = Stubby well zoned	629.8	5.7	.33	8
					MC2 = Elongate poorly zoned	614.0	5.2	.21	11
					MC3 = Elongate well zoned	601.1	6.5	.34	7

Note. $^{206}Pb/^{238}U$ ages of the entire suite and detailed zircon morphology descriptions are presented in Robinson et al. (2014).

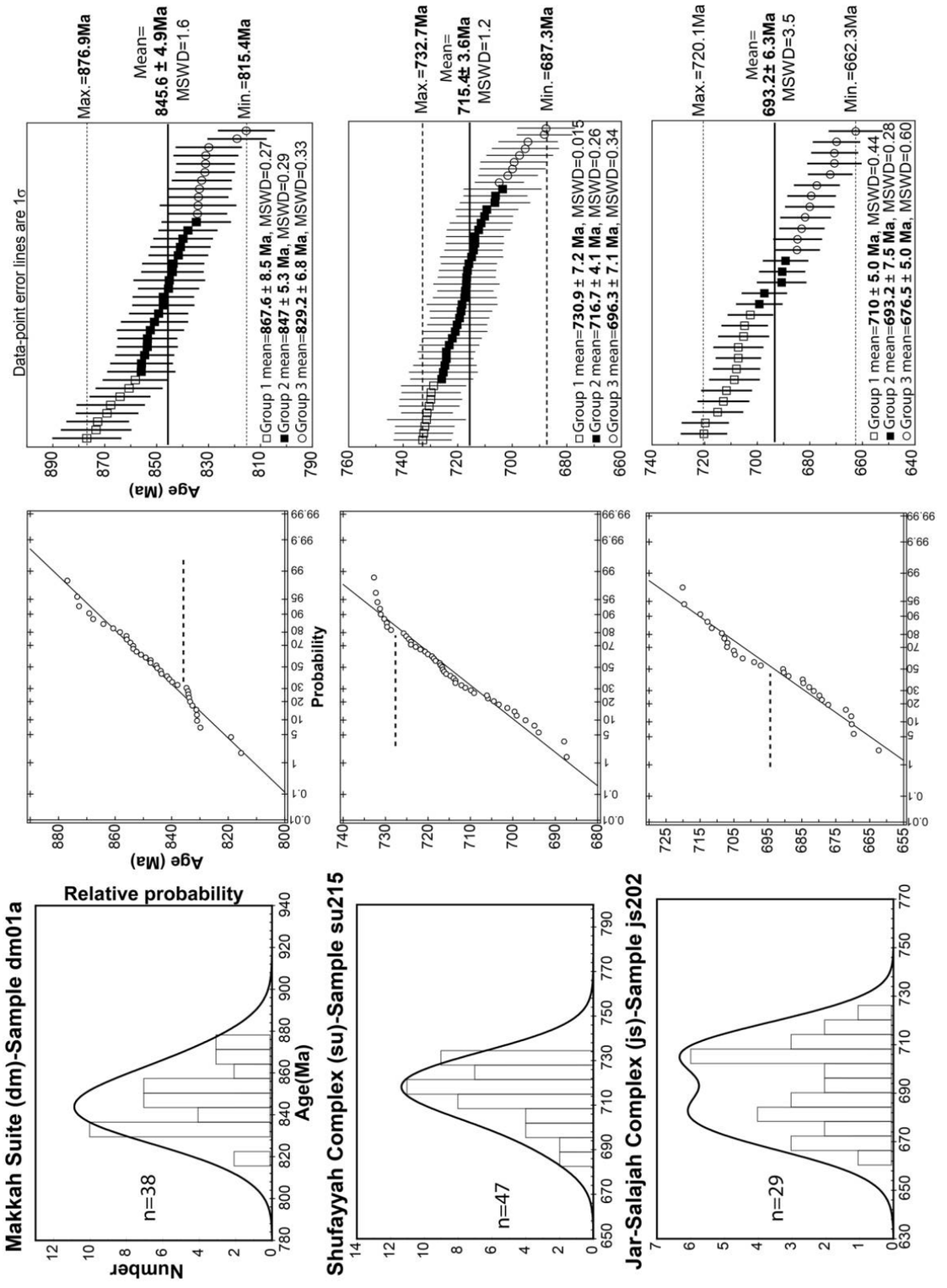

Figure 6. *Left*, probability distribution plots of Arabian granitoids. *Middle*, linearized plots highlighting data breaks and sideways distribution, suggesting the possibility of more than one age. *Right*, weighted average means of the three zircon morphology groups. These analyses have been numerically arranged in descending order to highlight the maximum and minimum values. The original randomly distributed analyses are presented in appendix D.

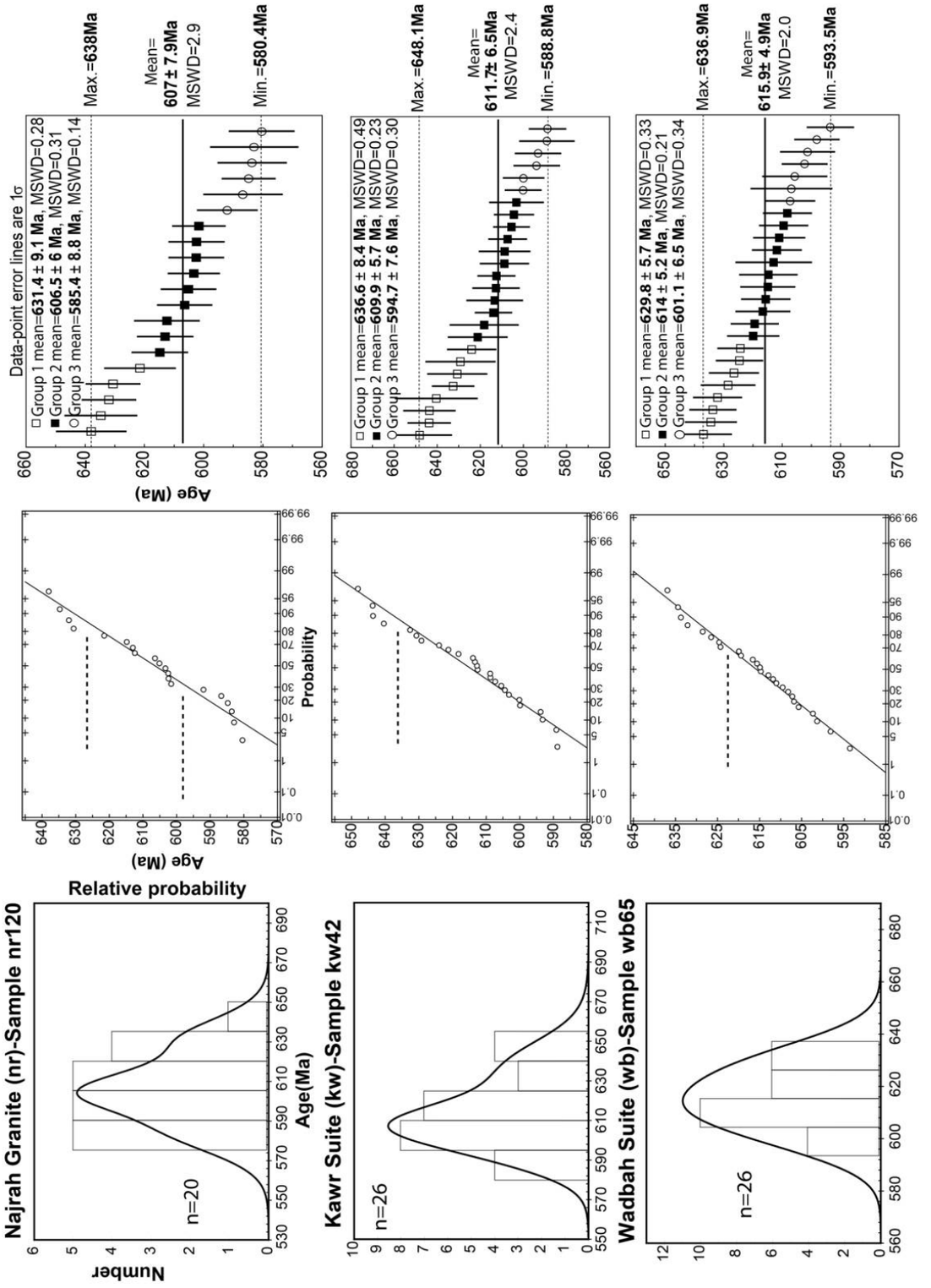

Figure 6 (*continued*)

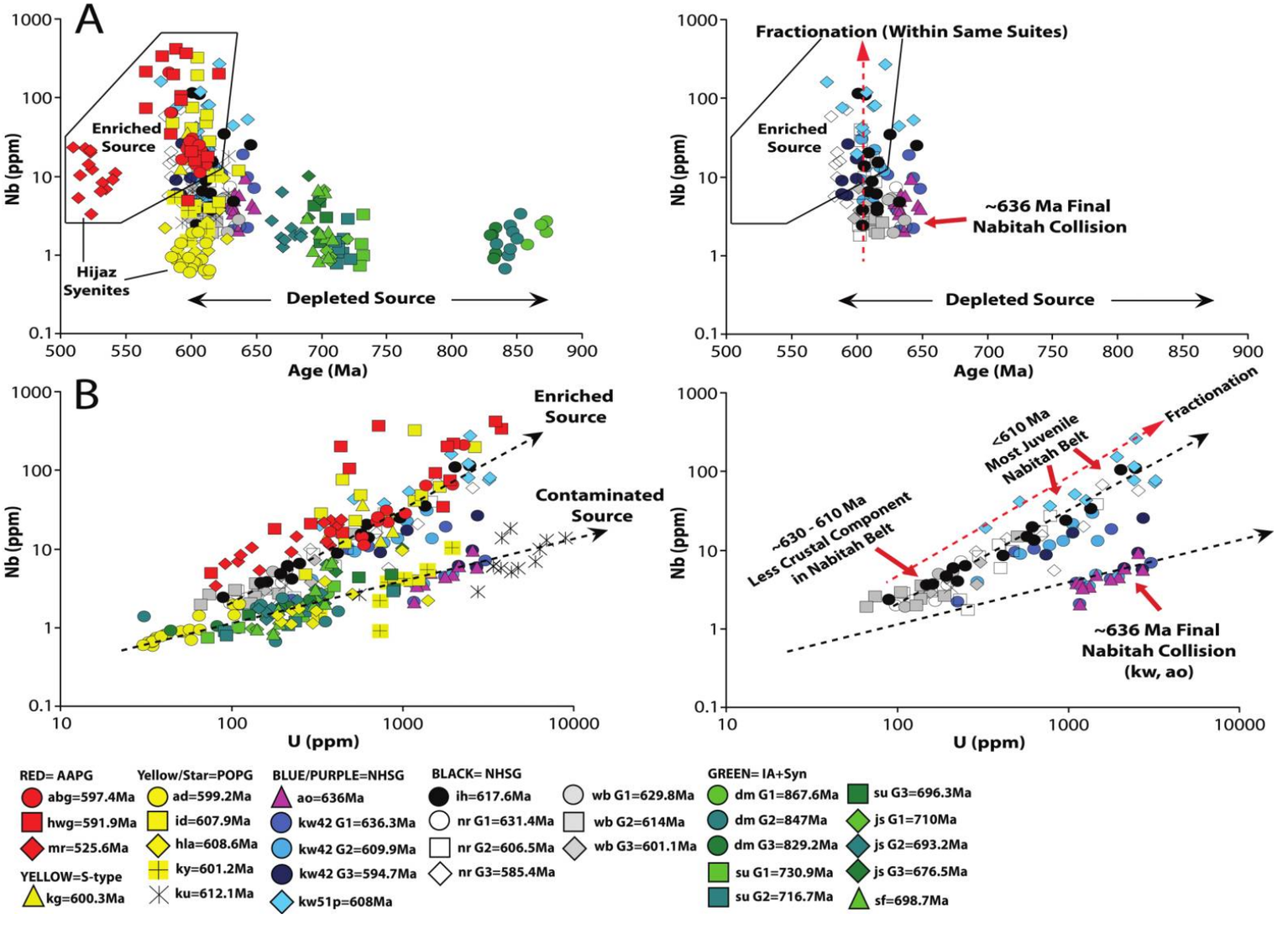

similarities, combined with identified discrete ages and similar spatial distributions (suture zones), suggest a link between island arc plus synorogenic I-type and postorogenic A-type sources. Following the recent studies of Robinson et al. (2014, 2015), these sources are derived from MORB-like and/or arc tholeiite–like geochemistry and are distinguished from the enriched, limited crust-mantle interaction of anorogenic A-type granites. To provide further evidence for this discrimination, the zircon geochemical properties and their relationship with whole-rock data from Robinson et al. (2015) will be discussed first. This will be followed by a discussion of the significance of the multiple discrete ages, and some plausible petrogenetic mechanisms will be suggested.

Contaminated and Enriched Mantle Sources beneath the Arabian Shield. Whole-rock data presented by Robinson et al. (2015) suggest the involvement of two distinct mantle sources in Arabian Shield granitoid generation using Nd isotopic signatures and Nb and Y trace elements. Robinson et al. (2015) suggest that island arc, synorogenic, and postorogenic I-S-A-type granites have intrasuite variation controlled by a combination of crustal assimilation of normal MORB (N-MORB)–like and/or arc tholeiite–like mafic parents and fractional crystallization in volcanic arc settings. By contrast, anorogenic A-type magmatism is enriched in HREE and incompatible elements (e.g., Nb, Rb, Ga, Nd, Zr, and Y) has limited crustal interaction, and is emplaced into within-plate and back-arc settings. Zircon geochemistry also supports the intrasuite variation and identification of two mantle sources (fig. 7). Zircon ages and corresponding Nb values separate the four magmatic groups and highlight a depleted parental source (low Nb) from ~850–600 Ma. This supports Robinson et al. (2015), who suggest that island arc, synorogenic, and postorogenic suites are derived from low incompatible MORB-like and/or arc tholeiite–like mafic parents. As illustrated in figure 7, these magmatic groups are isolated from the enriched source defined by the AAPGs. This change in source correlates well with the change in tectonic process described in Robinson et al. (2014).

As an example, the change in zircon source chemistry is pronounced between the zircons from the ~600 Ma Admar and the ~525 Ma Mardabah syenites (fig. 7). Both syenites reside in the Hijaz terrane (western Arabian Shield) and have similar petrographic and chemical properties (Robinson et al. 2015), but the ~525 Ma Mardabah zircons contain an order of magnitude greater Nb, suggesting a more enriched source. The zircon compositional field defined by the enriched mantle granitoids is also overlapped with zircons from the Nabitah and Halaban Sutures (Kawr, Wadbah, Ibn Hashbal, and Najirah Suites) and the northern end of the Arabian Shield (Idah Suite). When these trends are isolated into individual components, the Nabitah and Halaban Suture Granitoids (NHSG) illustrate a large range in Nb. This variation is present from the ~636 Ma final Nabitah collision (older zircon populations) and evolves to younger zircon populations with ~100 times the Nb concentration of the older populations within the same suite (fig. 7). The increase in Nb within the same suites is interpreted to resemble fractionation, which supports the whole-rock data from Robinson et al. (2015). This fractionation is also assumed to be the same for the highly evolved postorogenic perthitic (hypersolvus) A-type granitoids (POPG; e.g., Idah Suite), which is derived from a similar source to the POPG Admar syenite (i.e., MORB-type and/or arc tholeiite–type source).

The difference between the enriched and depleted sources and the extent of the fractionation within the NHSG suites are emphasized using Nb and Y (fig. 7). The zircon geochemistry defines two trends designated as enriched and contaminated sources in a manner similar to the Nb-versus-Y whole-rock data in Robinson et al. (2015). As illustrated in figure 7, the

Figure 7. *A*, Zircon geochemistry indicates multiple sources involved in Arabian Shield granitoids. This supports Robinson et al. (2015), who suggest that I-S-A-type granitoids from 850–600 Ma (green, yellow, black, blue/purple) are derived from mid-ocean ridge basalt–like and/or arc tholeiite–type sources followed by fractionation, while those from <600 Ma (red) are associated with an enriched source. This also coincides with the change in tectonic process at ~600 Ma described by Robinson et al. (2014). *B*, Zircon geochemistry defines two trends: (1) contaminated source defined by I-A-type granitoids with contaminated isotopic signatures in subduction settings (Robinson et al. 2015) and (2) enriched source defined by the most enriched A-type granites. The graph on the right isolates the A-type zircons associated with the sutures. It is suggested that an initial contamination at ~636 Ma (Kawr Suite, Al Hafoor Suite) is followed by a decrease in crustal component at ~630–610 Ma (Wadbah Suite, Najirah Granite, Ibn Hasbal Suite) and continued fractionation to the most juvenile zircons at <610 Ma (Kawr Suite, Najirah Granite). The G labels within the IA+Syn and postorogenic suites refer to the identified discrete morphologies/ages. Suite abbreviations are displayed in table 1. AAPG = <600 Ma anorogenic aegirine–bearing perthitic (hypersolvus) A-type granitoids; POPG = ~610–600 Ma postorogenic perthitic (hypersolvus) A-type granitoids; NHSG = ~640–585 Ma I- and A-type granitoids from the Nabitah and Halaban Suture; IA+Syn = ~870–675 Ma island arc and synorogenic I-type granitoids.

contaminated source trend is defined by the A-type Admar syenite (POPG), island arc and synorogenic I-type granitoids (IA+Syn), A-type Haml and Al Khushaymiyah Suites (POPG, Afif terrane), A-type Kawr and Al Hafoor Suites (NHSG, Asir-Afif collision), and finally the A-type Ar Ruwaydah Suite (NHSG, Ad Dawadimi-Halaban Suture). According to Robinson et al. (2015), these suites have isotopic signatures and geochemistry associated with crustal contamination of MORB and/or arc-tholeiite (REE-depleted) sources in volcanic arc settings; hence, the contaminated source trend. By contrast, the enriched trend is defined by enriched anorogenic aegirine–bearing perthitic (hypersolvus) A-type granitoid (AAPG) suites and fractionated NHSG A-type granites (fig. 7). Zircon geochemistry presented in this study also illustrates the decreasing crustal component beneath the Nabitah Suture. The ~636 Ma final collision of the Nabitah Suture is marked by the crustally contaminated Kawr and Al Hafoor Suite A-type granites (fig. 7). Following this, the lower limit of the enriched source trend is defined by the ~630–610 Ma Wadbah and Ibn Hashbal Suite A-type granites. It is suggested that these suites represent a decrease in the crustal component of the melt beneath the suture zone. With continued fractionation, the ~610 Ma A-types of the Kawr Suite appear and are the most juvenile end members beneath the suture (fig. 7). This process of decreasing crustal input in MORB and/or arc-tholeiite sources, in conjunction with remelting/fractionation (REE enrichment), may explain the overlap between enriched and contaminated A-type granites. However, it suggests that the enriched AAPG suites are not derived from the same source or petrogenetic mechanism, which is in agreement with the whole-rock data in Robinson et al. (2015) and the change in tectonic process at ~600 Ma from Robinson et al. (2014).

Magmatic Pulsing. A critical phenomenon found in the Arabian Shield geochronology is the separation of discrete magmatic ages and zircon morphologies within a given suite. This is found within the IA+Syn suites associated with accretion but also within NHSG A-type intrusions affiliated with the Nabitah and Halaban Sutures. Within each of these suites, the data typically span ~50 m.yr., which is a significant temporal window of magmatism considering the duration of other Arabian A-type activity (AAPG suites). Even if doubt is placed on discrete age separation, differences between zircon morphology and geochemistry are undeniable. It is therefore important to highlight the complex mingling field relationships observed in both IA+Syn (Makkah Suite) and NHSG (Kawr Suite) intrusions described in Robinson (2014). The former ranges from gabbro to granodiorite, while the latter ranges from gabbro to aegirine-bearing alkali granite. It would therefore be unsurprising if the samples reveal not only different geochemical parameters but also discrete zircon populations.

Given the discrete age and mingling evidence, there is still the possibility that the age differences are a function of inheritance or metamorphism. However, this is deemed unlikely because the ages of any country rocks surrounding the postorogenic intrusions are at least >50 m.yr. older and the IA+Syn suites are among the oldest granitoids in the Arabian Shield (with the exception of the Paleoproterozoic Khida terrane). Inheritance would likely be reflected in the U-Pb concordia as >50-m.yr. age gaps between zircon groups and/or Pb loss, but the discrete ages presented here are <20 m.yr. apart and exhibit no Pb loss (the Jar-Salajah Complex is possibly the exception). According to Robinson et al. (2014), all suites exhibit no age difference between cores and rims, as one might expect, which also rules out metamorphism. In addition, metamorphism is deemed very unlikely for the undeformed, postorogenic, aegirine-bearing alkali granites generated in extensional environments. It is possible that the youngest ages are simply inheritance (Pb loss) from older related magmatism within the same suite (e.g., Kawr Suite granite crystallization at 636.6 Ma, 609.9 Ma [inheritance], and 594.7 Ma [inheritance]); however, inherence in A-type magmatism is an undocumented phenomenon and regardless would still imply a long-lived magmatic event. It is therefore suggested that the IA+Syn and NHSG suites have multiple ages that represent discrete magmatic pulses within the same suite. A similar study was undertaken by Schaltegger et al. (2002), who explain multiple discrete ages and mantle sources within a given suite (Kohistan Island Arc, Pakistan) as the result of magmatic pulses. This is also found by Gagnevin et al. (2011), who investigated the Tuscan Magmatic Province, but the continuous magmatism expands only <3 m.yr.

I-Type Petrogenesis within Arabian Subduction Zones. According to Robinson et al. (2014), the island arc age magmatism of the Makkah Suite represents the initiation of western island arc magmatism in the Arabian Shield and reflects the eastward-subducting ocean plates of the East African Orogen (EAO; Stern 1994). As mentioned previously, the Makkah Suite has contaminated zircon and whole-rock geochemistry, which suggests the incorporation of a crustal component in the melt that generates these I-type granites (fig. 8). In addition, this suite exhibits multiple crystallization ages of ~867, ~847, and ~829 Ma, which are interpreted to resemble incremental subduction in an island arc and, farther abroad, the clo-

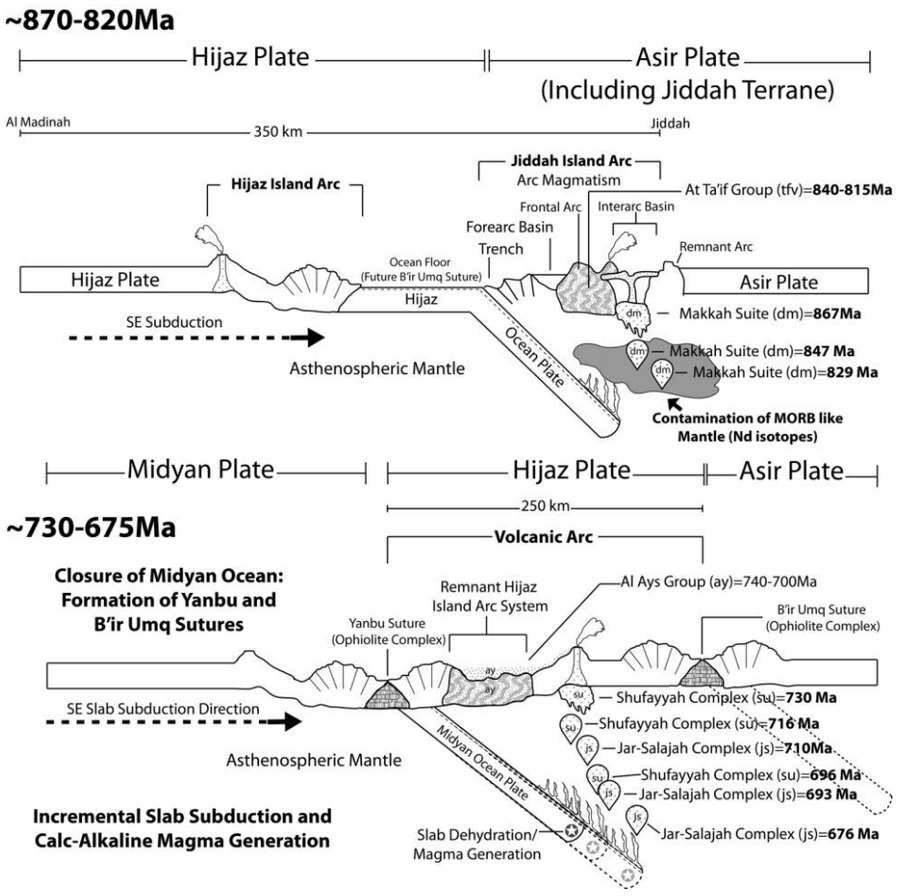

Figure 8. Tectonic model representing the island arc and synorogenic I-type magmatism in the western Arabian Shield, constructed using zircon geochemistry presented in this study and whole-rock geochemistry from Robinson et al. (2015). The Makkah Suite is the oldest unit dated from the sampled Arabian suites and is suggested to resemble incremental subduction in a contaminated island arc setting and closure of oceanic fragments in the East African Orogen. Farther north, the synorogenic magmatism of the Shufayyah and Jar-Salajah Complexes is interpreted to resemble the closure of these oceanic basins (evidenced by ophiolite sutures) and incremental calcalkaline subduction magmatism. MORB = mid-ocean ridge basalt.

sure of migrating ocean fragments in the EAO in incremental phases (Meert 2003; Li et al. 2008). The Makkah Suite is itself undeformed, but its three magmatic pulses are consistent with the timing of frontal arc rocks of the nearby At Ta'if Group (~840–815 Ma; Johnson 2006), which has low-grade (greenschist) metamorphism and westward-trending thrust kinematics (Robinson 2014).

Younger synorogenic I-type granitoids of the Shufayyah and Jar-Salajah Complexes (Hijaz terrane) intrude the ophiolite-decorated Yanbu Suture, which defines accretion between western terranes and eastward impingements of the EAO (Robinson et al. 2014). Calcalkaline subduction magmatism is initiated at ~730 Ma by the Shufayyah Complex and constrains the closure of the Yanbu Suture, which is in agreement with Johnson et al. (2011). This eastward-subducting plate produces another pulse at ~716 Ma, which is then followed by the generation of Jar-Salajah Complex at ~710 Ma in the same vicinity. The Shufayyah Complex produces one last pulse at ~696 Ma, and the Jar-Salajah Complex generates another two at ~693 and ~676 Ma. This series of magmatic pulses is again interpreted to represent incremental subduction and fractionation from slab-derived melts (fig. 8).

A-Type Petrogenesis beneath Arabian Sutures. The subtle differences between zircon morphology and contaminated zircon geochemistry trends presented in this article support the suggestion by Robinson et al. (2015) of a long-lived, lower crustal melting, assimilation, storage, and homogenization (MASH) zone (Smithies et al. 2011) below the Nabitah and Halaban Sutures. Following Flowerdew et al. (2013)

and Johnson (2006), it is suggested that the southern end of the Nabitah Suture is associated with extension and A-type magmatism, signifying the termination of microplate accretion at ~640 Ma. The data in this study support this, with the generation of the ~636 Ma Al Hafoor Suite and first magmatic pulse of the Kawr Suite. These two suites represent the initial melting of the lower crust (contaminated N-MORB and IAT mafic parents) that results from the influx of hot mantle via slab tear (fig. 9). This long-lived (~50 m.yr.) MASH zone undergoes continuous remelting and fractionation, which decreases the crustal component and taps off the first magmatic pulses of the ~630 and 614 Ma Wadbah Suite and the ~618 Ma Ibn Hashbal Suite (fig. 9). Continued remelting and fractionation produces another ~610 Ma Wadbah Suite pulse and the ~610 and ~594 Ma Kawr Suite pulses, which have the most juvenile and enriched geochemistry (fig. 9). Following this, the hot mantle influx providing the heat to the lower crust homogenizes and thermally relaxes, resulting in the termination of the lower crustal MASH zone. This model helps to explain the long-lived A-type magmatism beneath sutures and transition from contaminated, magnesian, volcanic arc granite (VAG) affinities of the early I-A-type end members to the juvenile, ferroan, within-plate granite (WPG) characteristics of the youngest end members within the same suite. In addition, this model also supports Flowerdew et al. (2013), who suggest a ~640 Ma tear in the Asir-Tathlith subduction zone.

East of the Afif terrane, westward subduction magmatism continued until after ~600 Ma in the Ar Ryan terrane (Doebrich et al. 2007; Cox et al. 2012). The long-lived lower crustal MASH model is assumed to be the petrogenetic mechanism for the Najirah Granite intruding the Halaban Suture. This A-type granite lies east of the ~615 Ma forearc sedimentary basin described in Cox et al. (2012) and has zircon and whole-rock geochemistry similar to the A-types in the Nabitah Suture. It is interpreted that the westward-subducting Ar Ryan terrane developed a slab tear at ~631 Ma, which generated the first magmatic pulse of the Najirah Granite from the lower crustal MASH zone. This contaminated melt continued to fractionate and produced the ~611 Ma Ar Ruwaydah Suite that intrudes the Najirah Granite. Following this, continued fractionation generated the second magmatic pulse of the Najirah Granite at ~606 Ma and finally another at ~585 Ma, which helps constrain the accretion age of the Halaban Suture and eastern Arabian Shield amalgamation (fig. 10). Other contaminated A-types, such as the Haml, Al Khushaymiyah, Idah, and Admar Suites (POPG), do not possess multiple crystallization ages. However, they have similar zircon and whole-rock geochemistry that is quite distinct from AAPG suites. It is therefore suggested that POPG suites are also generated by lower crustal melting in VAG settings but are not long-lived. It is possible that this short-lived A-type magmatism is related to the rate of hot mantle influx beneath the lower crust. This may be controlled by the extent of the tear and/or the angle of the subducting plate.

A-Type Petrogenesis within Back-Arc and Within-Plate Settings. The generation of <600 Ma AAPG suites in the Arabian Shield is consistent with a more enriched mantle source with limited crust-mantle interaction and coincides with the ~600 Ma final consolidation of the ANS (Collins and Pisarevsky 2005). According to Robinson et al. (2014), these suites are generated in back-arc and within-plate settings and indicate a change in tectonic process from older A-types associated with suture zones. Fortunately, the Midyan and Hijaz terranes in the western Arabian Shield provide an excellent example to explore this petrogenetic transition. As previously mentioned, the eastward-subducting Midyan plate generated the ~730–675 Ma contaminated VAG I-type magmatism emplaced into the Hijaz plate (conventional subduction-zone melting). Following this, the appearance of the ~600 Ma contaminated VAG A-type Admar syenite signifies ANS accretion cessation, and the resulting extension developed a tear in the Midyan plate ~75 m.yr. after I-type generation (fig. 11). There is also no reintroduction of calcalkaline magmatism following this A-type, which one would expect with a continued migrating slab. Farther north, the 597 Ma Al Bad Suite (WPG A-type batholith) is generated in a within-plate or back-arc setting in the Midyan plate with a distinctive enriched source (fig. 11). It is interpreted that the Al Bad Suite is the product of lithospheric delamination, which is discussed by Avigad and Gvirtzman (2009) as the petrogenetic mechanism for ~600 Ma ANS A-type granitoids. This enriched (ocean island basalt [OIB]–like) mantle is the result of extensive crustal thinning, lithospheric root removal, upwelling asthenospheric mantle, and thermal relaxation.

Lithospheric delamination is the preferred mechanism to explain the limited crust-mantle interaction and enriched source of the AAPG suites. It may be argued that AAPG suites are simply highly fractionated A-types generated in a manner similar to the most juvenile lower crustal MASH zone suites (e.g., the Kawr Suite), but this is deemed invalid. Zircon geochemistry presented in this study, combined with whole-rock data from Robinson et al. (2015), separate the highly fractionated A-types from enriched A-types, such as the Al Bad Suite. In addition,

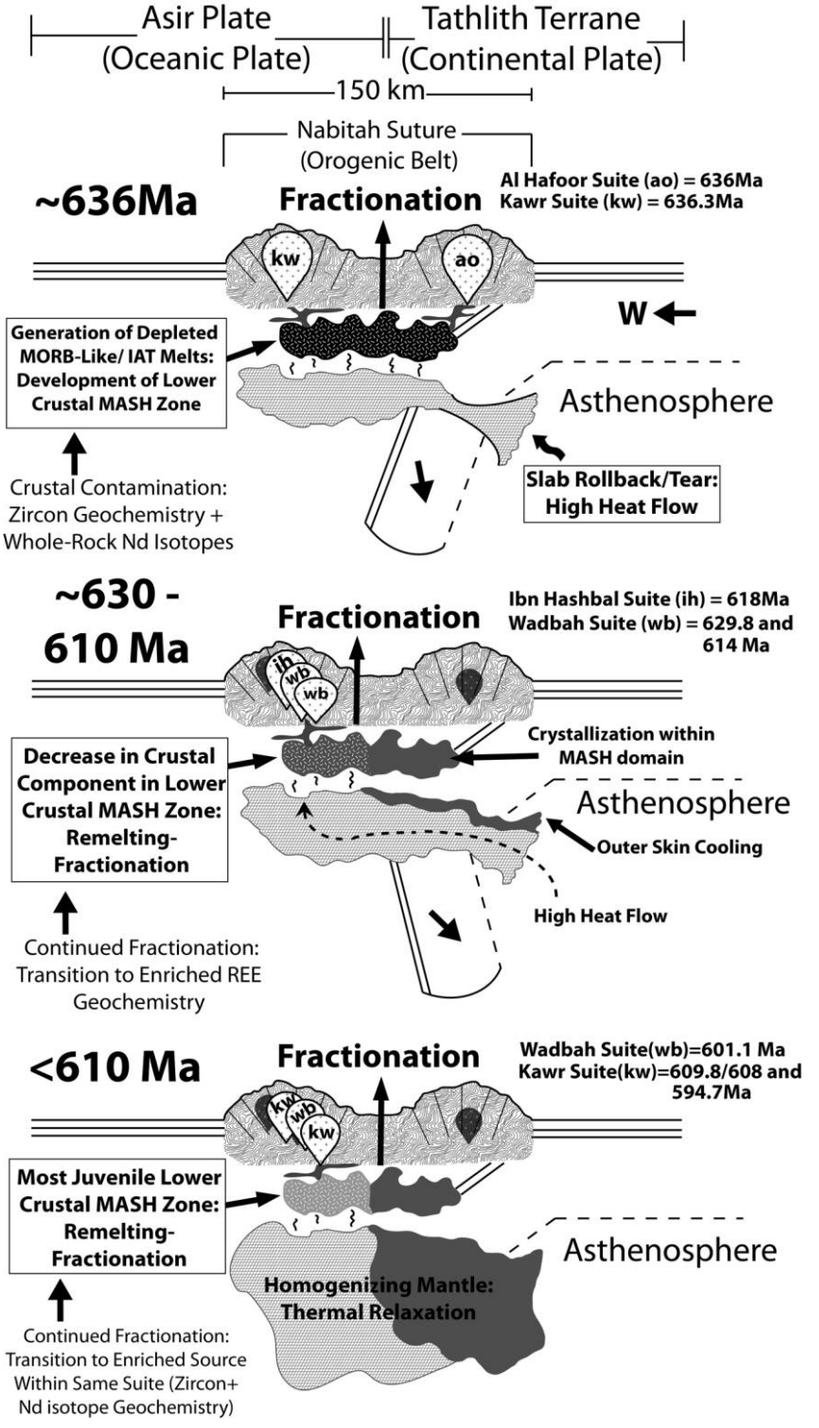

Figure 9. Tectonic model representing the Asir-Tathlith terrane A-type generation, constructed using zircon geochemistry presented in this study and whole-rock geochemistry from Robinson et al. (2015). The ~636 Ma Kawr and Al Hafoor Suites represent the initial tear in the subducting slab, which provides the heat influx to melt the lower crust beneath the Nabitah Suture and generate the lower crustal melting, assimilation, storage, and homogenization (MASH) zone. Remelting and fractionation decreases the crustal component within this zone and produces the younger Ibn Hashbal and Wadbah Suite magmatic pulses. Following this, continued fractionation produces the most juvenile and rare earth element (REE)–enriched A-types, correlating with the final pulses of the Wadbah and Kawr Suites. MORB = mid-ocean ridge basalt; IAT = island arc tholeiite.

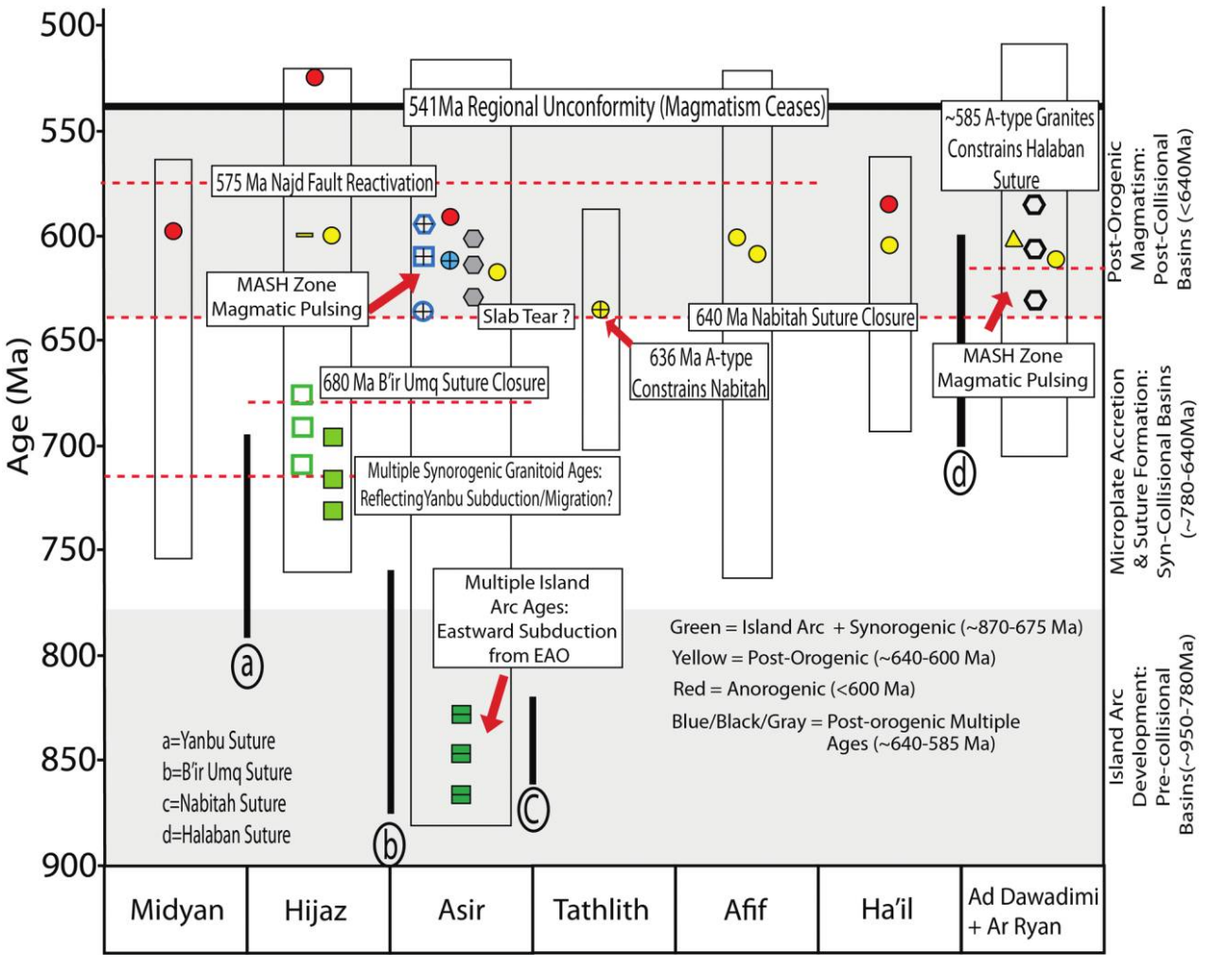

Figure 10. Time-space plot modified from Robinson et al. (2015) highlighting the spatial relationship and mechanisms of the four tectonic groups sampled in the Arabian Shield. The age range boxes in each terrane are compiled from an Arabian-Nubian Shield data set presented in Robinson et al. (2014). Note the multiple crystallization ages associated with I- and A-type granites generated within subduction settings (island arc plus synorogenic) or beneath suture zones immediately following extension (postorogenic). Dashes = gabbro; squares = I-type granite; triangles = S-type granite; circles = hypersolvus A-type granite; hexagon = hypersolvus aegirine–bearing A-type granite. Dashes inside squares and crosses inside circles/hexagons represent suites with gabbroic and gabbroic/dioritic/monzonitic samples, respectively. MORB = mid-ocean ridge basalt; EAO = East African Orogen.

the ~525 Ma Mardabah syenite (located in the Hijaz terrane next to the contaminated ~600 Ma Admar syenite) has the same enriched source as the Al Bad Suite and is associated with localized crustal extension (Robinson et al. 2014). It is assumed that if allowed to continue to fractionate, these syenites would produce the same isotopic and geochemical properties as the more evolved A-types in their respective fields.

Both contaminated and enriched A-types result from regional extension, but their petrogenetic mechanisms differ (i.e., slab tear/lower crustal melting vs. within-plate delamination). This change in tectonic process at ~600 Ma appears to complement Be'eri-Shlevin et al. (2010) and Stoeser and Frost (2006), who propose a more depleted mantle beneath the ANS influenced by pre-Neoproterozoic crust, but also Stein and Goldstein (1996) for an enriched mantle. Although these data cannot rule out ~600 Ma mantle enrichment created by upwelling plumes that can be geochemically traced back to ~1000 Ma (Stein and Goldstein 1996), it does not substantiate this mechanism for ANS magmatism between ~845 and 600 Ma. Instead, this study suggests subduction and accretion between ~845 and 600 Ma involving contaminated MORB-like and/or arc tholeiite–like magmatism, slab tear, and melting of the lower crust. This is then followed by lithospheric delamination

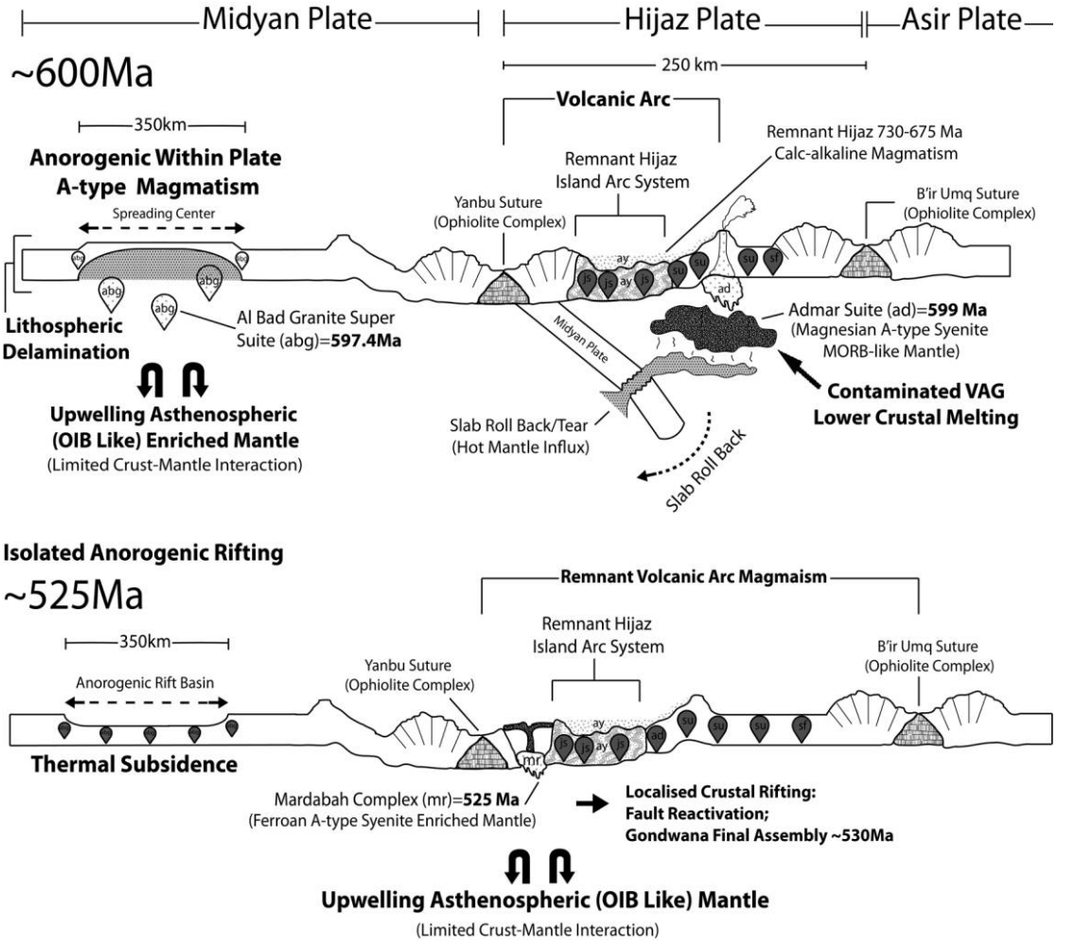

Figure 11. Tectonic model representing the postorogenic and anorogenic magmatism in the western Arabian Shield, constructed using zircon geochemistry presented in this study and whole-rock geochemistry from Robinson et al. (2015). The ~599 Ma Admar Suite is a magnesian-rich A-type syenite associated with extension and slab tear resulting in lower crustal melting of a mid-ocean ridge basalt (MORB)–like source above the Hijaz plate. Farther north, the ~597 Ma Al Bad batholith is a ferroan A-type granite associated with an enriched source and limited crust mantle generated by within-plate lithospheric delamination. The ~525 Ma Mardabah Complex syenite is also a within-plate A-type associated with the same enriched mantle source, but its age and isolated nature suggest localized extension possibly linked to final Gondwana assembly (Robinson et al. 2014). OIB = ocean island basalt; VAG = volcanic arc granite.

associated with upwelling enriched mantle (OIB-like) confined to within-plate and back-arc settings, which is in agreement with Avigad and Gvirtzman (2009).

Conclusions

Arabian Shield igneous zircon geochemistry indicates that both contaminated and enriched mantle sources are involved in Arabian Shield evolution. Overall, zircon geochemistry distinguishes and supports four magmatic groups defined in Robinson et al. (2015): (1) ~870–675 Ma island arc and synorogenic granitoids (IA+Syn), (2) ~640–585 Ma granitoids from the Nabitah and Halaban Suture (NHSG), (3) ~610–600 Ma postorogenic perthitic (hypersolvus) granitoids (POPG), and (4) <600 Ma anorogenic aegirine–bearing perthitic (hypersolvus) granitoids (AAPG). Groups 1, 2, and 3 include suites ranging from I-S- to A-type granites that have parental magmas with low Nb contents (~1 ppm) and fractionate toward high Nb values (~300 ppm). These also possess intrasuite variation within LREE and HREE signatures and define the contaminated source trend utilizing Nb and U trace elements. By contrast, group 4 suites have parental magmas that are enriched in Nb with lowest and highest values of ~10 and 400 ppm, respectively, and define the enriched source trend associ-

ated with limited crust-mantle interaction. These contaminated and enriched source trends support the whole-rock Nb-versus-Y trends described in Robinson et al. (2015).

Discrete zircon morphologies and U-Pb ages are identified within the IA+Syn I-type and NHSG A-type granites, which exhibit extensive magma mingling. These are interpreted as discrete crystallization ages reflecting magmatic pulsing from contaminated MORB-like and/or arc tholeiite–like mantle. It is suggested that IA+Syn I-type granitoids reflect lower crustal melting within typical VAG settings and incremental subduction of eastward-migrating oceanic fragments in the EAO. This process of lower crustal melting and eastward migration is initiated in the Asir terrane by the Makkah Suite (~867, ~847, and ~829 Ma). Younger synorogenic calcalkaline magmatism correlating to the Shufayyah (~730, 716, and 696 Ma) and Jar-Salajah (~710, 693, and 676 Ma) Complexes is suggested to define the accretion of the western terranes with eastern components of the EAO. The appearance of ~640 Ma A-type magmatism within suture zones (NHSG suites) is a response to the onset of extension at the termination of orogenesis. These A-type suites illustrate a transition from contaminated mantle (~636 Ma) to enriched mantle with a decrease in crustal input (~630–610 Ma) and finally to juvenile, enriched mantle with limited crustal interaction (<610 Ma). This long-lived A-type magmatism with multiple age groups is interpreted to resemble an initial slab tear associated with slab rollback and the development of a lower crustal MASH zone via hot mantle influx. The subsequent magmatic pulses emitted ~20 m.yr. apart from this MASH zone become increasingly more juvenile by remelting and fractionation. This process accounts for the transition from magnesian-rich VAG end members to ferroan-rich WPG end members within the same suite. The appearance of enriched AAPG suites (<600 Ma) in within-plate or back-arc settings is consistent with the final collision of Neoproterozoic India with the African continents as central Gondwana formed (Robinson et al. 2014). The Midyan and Hijaz terranes illustrate the transition of A-type magmatism associated with lower crustal melting and slab tear (POPG) to A-type magmatism generated by within-plate lithospheric delamination and asthenospheric upwelling. Lithospheric delamination can account for the short-lived (<20 m.yr.) A-type magmatism associated with limited crust-mantle interaction and enriched geochemistry presented both in this study and in Robinson et al. (2015).

ACKNOWLEDGMENTS

The Saudi Geological Survey—in particular, K. Kadi and M. M. Nahdi—is thanked for providing research funding and gracious hospitality in Saudi Arabia during February 2010 fieldwork. B. Wade and A. Netting from Adelaide Microscopy are also thanked for help in obtaining zircon geochemistry and geochronology. P. Johnson is greatly appreciated for his contributions to ANS data interpretation. A. S. Collins acknowledges funding from the Australian Research Council Future Fellowship Scheme (project FT120100340). This article forms Centre for Tectonics, Resources and Exploration record 326 and is a contribution to International Geoscience Programme (IGCP) project 628.

REFERENCES CITED

Avigad, D., and Gvirtzman, Z. 2009. Late Neoproterozoic rise and fall of the northern Arabian-Nubian Shield: the role of lithospheric mantle delamination and subsequent thermal subsidence. Tectonophysics 477:217–228.

Azer, M. K., and Farahat, E. S. 2011. Late Neoproterozoic volcano-sedimentary successions of Wadi Rufaiyil, southern Sinai, Egypt: a case of transition from late- to post-collisional magmatism. J. Asian Earth Sci. 42:1187–1203.

Be'eri-Shlevin, Y.; Katzir, Y.; Blichert-Toft, J.; Kleinhanns, I. C.; and Whitehouse, M. J. 2010. Nd-Sr-Hf-O isotope provinciality in the northernmost Arabian-Nubian Shield: implications for crustal evolution. Contrib. Mineral. Petrol. 160:181–201.

Belousova, E. A.; Griffin, W. L.; and O'Reilly, S. Y. 2006. Zircon crystal morphology, trace element signatures and Hf isotope composition as a tool for petrogenetic modelling: examples from eastern Australian granitoids. J. Petrol. 47:329–353.

Bentor, Y. K. 1985. The crustal evolution of the Arabo-Nubian Massif with special reference to the Sinai Peninsula. Precambrian Res. 28:1–74.

Black, R., and Liegeois, J.-P. 1993. Cratons, mobile belts, alkaline rocks and continental lithospheric mantle: the Pan-African testimony. J. Geol. Soc. 150:89–98.

Collins, A. S., and Pisarevsky, S. A. 2005. Amalgamating eastern Gondwana: the evolution of the Circum-Indian Orogens. Earth Sci. Rev. 71:229–270.

Cox, G. M.; Lewis, C. J.; Collins, A. S.; Halverson, G. P.; Jourdan, F.; Foden, J.; Nettle, D.; and Kattan, F. 2012. Ediacaran terrane accretion within the Arabian-Nubian Shield. Gondwana Res. 21:341–352.

Doebrich, J. L.; Al-Jehani, A. M.; Siddiqui, A. A.; Hayes, T. S.; Wooden, J. L.; and Johnson, P. R. 2007. Geology and metallogeny of the Ar Ryan terrane, eastern Arabian Shield: evolution of a Neoproterozoic continental-margin arc during assembly of Gondwana within the East African Orogen. Precambrian Res. 158:17–50.

Eyal, M.; Litvinovsky, B.; Jahn, B. M.; Zanvilevich, A.; and Katzir, Y. 2010. Origin and evolution of post-collisional magmatism: coeval Neoproterozoic calc-alkaline and alkaline suites of the Sinai Peninsula. Chem. Geol. 269:153–179.

Flowerdew, M. J.; Whitehouse, M. J.; and Stoesser, D. B. 2013. The Nabitah fault zone, Saudi Arabia: a Pan-African suture separating juvenile oceanic arcs. Precambrian Res. 239:95–105.

Frost, C. D., and Frost, B. R. 2011. On ferroan (A-type) granitoids: their compositional variability and modes of origin. J. Petrol. 52:39–53.

Gagnevin, D.; Daly, J. S.; Horstwood, M. S. A.; and Whitehouse, M. J. 2011. In-situ zircon U-Pb, oxygen and hafnium isotopic evidence for magma mixing and mantle metasomatism in the Tuscan Magmatic Province, Italy. Earth Planet. Sci. Lett. 305:45–56.

Griffin, W. L.; Powell, W. J.; Pearson, N. J.; and O'Reilly, S. Y. 2008. GLITTER: data reduction software for laser ablation ICP-MS. *In* Sylvester, O., ed. Laser ablation–ICP-MS in the earth sciences. Mineralogical Association of Canada Short Course Series 40:204–207. Appendix 2.

Grimes, C. B.; John, B. E.; Cheadle, M. J.; Mazdab, F. K.; Wooden, J. L.; Swapp, S.; and Schwartz, J. J. 2009. On the occurrence, trace element geochemistry, and crystallisation history of zircon from in situ ocean lithosphere. Contrib. Mineral. Petrol. 158:757–783.

Gvirtzman, Z., and Nur, A. 1999. The formation of Mount Etna as the consequence of slab rollback. Nature 401:782–785.

Hoskin, P. W. O., and Schaltegger, U. 2003. The composition of zircon and igneous and metamorphic petrogenesis. Rev. Mineral. Geochem. 53:27–62.

Jenner, F. E., and O'Neil, H. C. 2012. Analysis of 60 elements in 616 ocean floor basaltic glasses. Geochem. Geophys. Geosyst. 13:1–11.

Johnson, P. R. 2006. Explanatory notes to the map of Proterozoic geology of western Saudi Arabia. Technical Report, Saudi Geological Survey, SGS-TR-2006-4/1427H 2006 G.

Johnson, P. R.; Andersen, A.; Collins, A. S.; Fowler, A. R.; Fritz, H.; Ghebreab, W.; Kusky, T.; and Stern, R. J. 2011. Late Cryogenian–Ediacaran history of the Arabian-Nubian Shield: a review of depositional, plutonic, structural, and tectonic events in the closing stages of the northern East African Orogen. J. Afr. Earth Sci. 10:1–179.

Li, Z. X.; Bogdanova, S. V.; Collins, A. C.; Davidson, A.; De Waele, B.; Ernst, R. E.; Fitzsimons, I. C. W; et al. 2008. Assembly, configuration and break-up history of Rodinia: a synthesis. Precambrian Res. 160:179–210.

Ludwig, K. R. 2000. Isoplot/Ex version 2.2: a geochronological toolkit for Microsoft Excel. Berkeley Geochronology Center Special Publication 1a. Berkeley, CA, Berkeley Geochronology Center.

Meert, J. G. 2003. A synopsis of events related to the assembly of eastern Gondwana. Tectonophysics 362:1–40.

Melnykov, V., and Maitra, R. 2010. Finite mixture models and model-based clustering. Stat. Surv. 4:80–116.

Nettle, D.; Halverson, G. P.; Cox, G. M.; Collins, A. S.; Schmitz, M.; Gehling, J.; Johnson, P. R.; and Kadi, K. 2014. A Middle-Late Ediacaran volcano-sedimentary record from the eastern Arabian-Nubian Shield. Terra Nova 26:120–129.

Norman, M. D.; Pearson, N. J.; Sharma, A.; and Griffin, W. L. 1996. Quantitative analysis of trace elements in geological materials by laser ablation ICPMS: instrumental operating conditions and calibration values of NIST glasses. Geostand. Newsl. 20:247–261.

Pupin, J. P. 1980. Zircon and granite petrology. Contrib. Mineral. Petrol. 73:207–220.

Robinson, F. A. 2014. Geochronological and geochemical constraints on the lithospheric evolution of the Arabian Shield, Saudi Arabia: understanding plutonic rock petrogenesis in an accretionary orogen. PhD dissertation, University of Adelaide.

Robinson, F. A.; Foden, J. D.; and Collins, A. S. 2015. Geochemical and isotopic constraints on island arc, synorogenic, post-orogenic and anorogenic magmatism in the Arabian Shield, Saudi Arabia. Lithos 220–223:97–115.

Robinson, F. A.; Foden, J. D.; Collins, A. S.; and Payne, J. L. 2014. Arabian Shield magmatic cycles and their relationship with Gondwana assembly: insights from zircon U-Pb and Hf isotopes. Earth Planet. Sci. Lett. 408:207–225.

Sambridge, M. S., and Compston, W. 1994. Mixture modelling of multi-component data sets with application to ion-probe zircon ages. Earth Planet. Sci. Lett. 128:373–390.

Schaltegger, U.; Zeilinger, G.; Frank, M.; and Burg, J.-P. 2002. Multiple mantle sources during island arc magmatism: U-Pb and Hf isotopic evidence from the Kohistan arc complex, Pakistan. Terra Nova 14:461–468.

Smithies, R. H.; Howard, H. M.; Evins, P. M.; Kirkland, C. L.; Kelsey, D. E.; Hand, M.; Wingate, M. T. D.; Collins, A. S.; and Belousova, E. 2011. High-temperature granite magmatism, crust-mantle interaction and the Mesoproterozoic intercontinental evolution of the Musgrave Province, Central Australia. J. Petrol. 52:931–958.

Stein, M., and Goldstein, S. L. 1996. From plume head to continental lithosphere in the Arabian-Nubian Shield. Nature 382:773–778.

Stern, R. J. 1994. Arc assembly and continental collision in the Neoproterozoic East African Orogen: implications for the consolidation of Gondwanaland. Annu. Rev. Earth Planet. Sci. 22:319–351.

Stoeser, D. B., and Camp, V. E. 1985. Pan-African microplate accretion of the Arabian Shield. Geol. Soc. Am. Bull. 96:817–826.

Stoeser, D. B., and Frost, C. D. 2006. Nd, Pb, Sr and O isotopic characterisation of Saudi Arabian Shield terranes. Chem. Geol. 226:163–188.

Sun, S.-S., and McDonough, W. F. 1989. Chemical and isotopic systematics of oceanic basalts: implications for mantle composition and processes. Geol. Soc. Spec. Publ. 42:313–345.

Turner, S.; Foden, J.; and Morrison, R. S. 1992. Derivation of some A-type magmas by fractionation of basaltic magma: an example from the Padthaway Ridge, South Australia. Lithos 28:151–179.